QATAR UNIVERSITY

COLLEGE OF ARTS AND SCIENCES

NITROGEN AND SULFUR– DOPED CARBON NANOFIBER MIXED OXIDES COMPOSITES FOR SUPERCAPACITOR APPLICATIONS

BY

ABDULLAH AL ASHRAF

A Thesis Submitted to the Faculty of

College of Arts and Sciences

in Partial Fulfillment

of the Requirements

for the Degree of

Master of Science in

Materials Science and Technology

June, 2016

Committee

The members of the Committee approve the thesis of Abdullah Al Ashraf defended on 26/5/2016.

_____
Dr. Ahmed Elzatahry
Thesis/Dissertation Supervisor

_____
Dr. Talal Altahtamouni
Committee Member

_____
Dr. Nasr Bensalah
Committee Member

_____
Dr. Ilias Belharouk
Committee Member

_____
Dr. Abdul Shakoor
Committee Member

Approved:

_____

Dr. Eiman Mustafawi, Dean, College of Arts and Sciences

Abstract

Energy storage devices including supercapacitor are among the rapidly growing field of alternatives for rechargeable batteries due to its high energy density and long life cyclability performance. Electrospinning is a versatile process that produces polymer fibers. The diameter of these fibers ranges from micrometers to few nanometers. In this work, we aimed to synthesize Carbon nanofibers (CNF) from these polymer fibers by employing annealing (high temperature heat treatment). The fibers were doped with nitrogen (N) and/or sulfur (S) source during electrospun fibers fabrication. Later, the N and/or S doped CNF were loaded with mixed metal oxide e.g. Ni, Sn, and Ru by microwave technique. We characterized and investigated these materials and measured their performance for supercapacitor applications. Metal loaded 1 wt. % Thiourea doped (M-CNF-T-1%) sample electrodes showed a high specific capacitance value of 207.29 F. g^{-1} at scan rate of 10 mVs^{-1}. This was ascribed to improved electrical conductivity and ion permittivity of carbon materials due to the presence of graphitic-nitrogen on carbon ring structure and nature of catalyst used. Hence, the synthesized materials represents as suitable electrode materials for high-performance supercapacitors.

Table of contents

List of Tables

List of Figures

Abbreviation

AAI: Iron acetylacetonate

ACNF: Activated Carbon Nanofiber

AAC/MnO_2: Iron acetylacetonate MnO_2

CNF: carbon nano fibers

C_S: Specific capacitance

ECBs: Electrochemical batteries

EDLC: Electrical double layer capacitance

GACNF: Graphitized Activated Carbon Nanofiber

HESS: Hybrid battery-supercapacitor

MOs: Metal oxides

PC: Pseudo capacitors

PIM: Polymer of intrinsic micro porosity

PMHS: Polymethylhydrosiloxane

PAN: Polyacrylonitrile

PI: Polyimide

PVP: Polyvinylpyrrolidone

PMMA : Poly(methyl methacrylate)

PS: Phenylsilane

PPy: Polypyrrole

PAN-co-PB: poly(acrylonitrile-co-butadiene)

SCs: Supercapacitors

Acknowledgements

The present work was carried out between 2015 and 2016 at the College of Arts and Sciences at Qatar University under the supervision of Prof. Ahmed Elzatahry.

First of all, I would like to thank my main supervisor, Prof. Ahmed Elzatahry for his guidance, support and encouragement in this research work. I am, sincerely grateful for the information provided, helpful discussions, kindness and patience during the research period.

My sincere appreciation goes to Dr. Nasr Bensalah from Department of Chemistry and Earth Sciences, Dr. Talal Altahtamouni from Master of Material Science program, Dr. Abdul Shakoor from Center for Advanced Materials and Dr. Ilias Belharouk who co-supervised this work and were at any time, willing to spare their time to encourage and discuss with me the subject matter. I am thankful for their advice and active guidance.

Similarly, my appreciation goes to supportive staff (Dr. Peter Kasak, Dr. Noora Al-Thani, Dr, Jolly, Mostafa Hussein, Ahmed Bahgat, Abdul Jaleel) at the Center of Advanced Materials (CAM) and Material Science and Technology Program at Qatar University particularly Dr. Aboubakr Ali, for his support every time when needed.

A special thank goes to Dr. Yahia Shuaib, Post-Doctoral Researcher from Department of Chemistry and Earth Science, for giving me the opportunity to carry out experiments on their devices. Also, I would like to express my gratitude for the support of their research team.

I would like to thanks Dr. Abdullah Al-Enaizi, Assistant Prof. of Chemistry at King Saud University (KSU), for his support to carry out a part of my research work at their lab. A special thanks goes to Mr. Meera and Mr. Kamal for their assistance during the experimental work at KSU.

I am deeply grateful to all people and colleagues from Material Science and Technology Master's Program who gave me warm welcome to their group and have since been my friends. Specifically, I am very thankful to Mrs. Sharon Sonia, who took care of administrative concerns anytime I asked for her assistance and Mr. Jaleelur Rahman for supporting the laboratory works.

Finally, I would like to thank my parents and family for their love, support, understanding and optimism and encouragement during these years. I really appreciate it.

Motivation

It is important to highlight that, this research represents good initiative collaboration between College of Arts and Science and Center for Advanced Materials at Qatar University. This collaboration will open profound new opportunities for students, faculties and researchers for scientific cooperation to solve real and actual problems, and will strengthen the partnership between the research center and college.

This work opens a new path for incoming students to work on energy related field, which is very innovative emerging field of research in Qatar. This work could be considered as a part of accomplishment of Qatar's National Vision 2030.

Chapter 1

1. Introduction

Energy storage devices, including electrochemical supercapacitors, are gaining extensive research interest due to rapid population growth, fear of exhaustion of fossil fuels, and the pressing needs for efficient energy storage schemes for miniature to grid level appliances. Energy generated by some of the newer but renewable sources, for example, solar and wind power requires converting energy to store for later use, so an energy storage system is a must. The development of supercapacitor devices is becoming progressively more essential in order to meet global needs. The development of new materials for supercapacitor devices could be an effective means for energy storage, and hence plays an essential role to reach this objective.

Electrode materials are the crucial parts for supercapacitor devices which control the charge storing and carriage system (T. Chen & Dai, 2013). Porous carbon having high surface area, and various metal oxide/ hydroxide of transition elements, conducting polymers is extensively used as supercapacitor's electrode materials (He et al., 2013). However, the performance greatly depends on the materials used in the construction of the device.

An extensive variety of preparation methods are available for the preparation of electrode materials, among which the electrospinning process is foremost due to its convenient processability, uniform dispersity of active materials, operational flexibility, mass productivity and possibility of producing free-standing flexible materials (Al-Enizi et al.,

2014), (S Chen, He, & Hou, 2013). Electrospinning based carbon materials influence the performance of the supercapacitor by improving the specific surface area, surface chemical properties, conductivity, pore structure with appropriate size, and their distribution (Zeng et al., 2015), (Bhagwan, Sahoo, Yadav, & Sharma, 2015). Polymer fibers are primarily fabricated by electrospinning polymer solutions, taken after by stabilizing at temperature of 200- 275 ºC and carbonizing at 800-1000 ºC or more, resulting in carbon fibers (Beese, Papkov, Li, Dzenis, & Espinosa, 2013).

The performance of the carbon materials for supercapacitor applications is further improved by doping of heteroatoms. Heteroatoms are specified as any atoms (S, N, O, P, B) rather than carbon or hydrogen in the skeleton of the molecular structure of graphite ring. Due to the addition of heteroatoms, chemical properties of the surface improve, which further promote pseudo-capacitance and wettability of the electrodes by the formation of reversible redox reactions (Tian et al., 2015), (B. H. Kim, Seung Yang, & Woo, 2013).

Furthermore, loading metal oxide/ hydroxide on carbon materials enhances the performance i.e. specific capacitance value, for supercapacitor materials. Among other techniques, microwave assisted metal loading is thought to be an eco-friendly, fast, efficient and uniform heating method (Lisong Chen et al., 2015).

Among different strategies, microwave helped metal stacking is thought to be an ecologically well disposed, quick and vitality successful strategy Synthesis of nanomaterials by this technique is more favorable and easily achievable than heating in a

conventional furnace due to the uniform distribution of heating within a short time (Lisong Chen et al., 2015).

Hence, a novel route preparation method of doped carbon materials, based on the electrospinning process combined with metal oxide/ hydroxide loading by microwave technique, provides the ability to produce high performance supercapacitor materials which could play a promising role as a future energy storage device.

1.1 Working principles of the supercapacitor

An electrochemical capacitor, or supercapacitor, is comprise of two electrodes. One works as positive or cathode and the other as negative or anode. A separator separates both electrodes which acts as an ion-permeable membrane. The construction of the device is completed by adding the electrolyte which ionically connected the two electrodes. When an applied voltage polarizes the electrodes, opposite charge form on the electrode surface due to the electric double layer circumstance. For instance, the positive ions will accumulate on the negatively charged electrode at electrolyte/electrode interface. Figure 1.1 shows the schematics of basic components of supercapacitor.

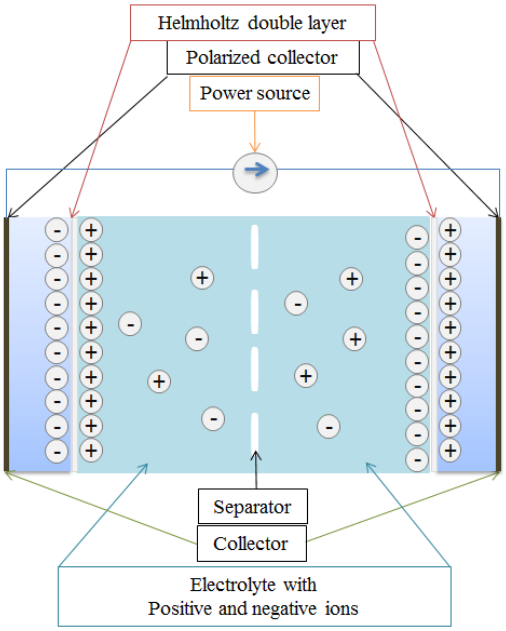

Figure 1.1: Schematic drawing of basic components of supercapacitor

All electrochemical capacitors are based on the principles of two main concept according to the charge storage mechanism (Candelaria et al., 2012), namely, electrochemical double layer capacitance (EDLCs) and pseudo capacitance (PCs). The electrical energy which is stored and released by EDLCs is a non-faradic reaction. The reaction usually happens between the electrolyte and the electrode's surface, is a very fast reaction, and shows good stability. As a result, EDLC shows long time cyclability and high capability rate by providing low specific capacitance. PCs based on redox faradic reaction occur also between electrode and electrolyte surface, providing high specific capacitance but short cyclability and power density. Figure 1.2 represents the schemetics of supercapacitor types.

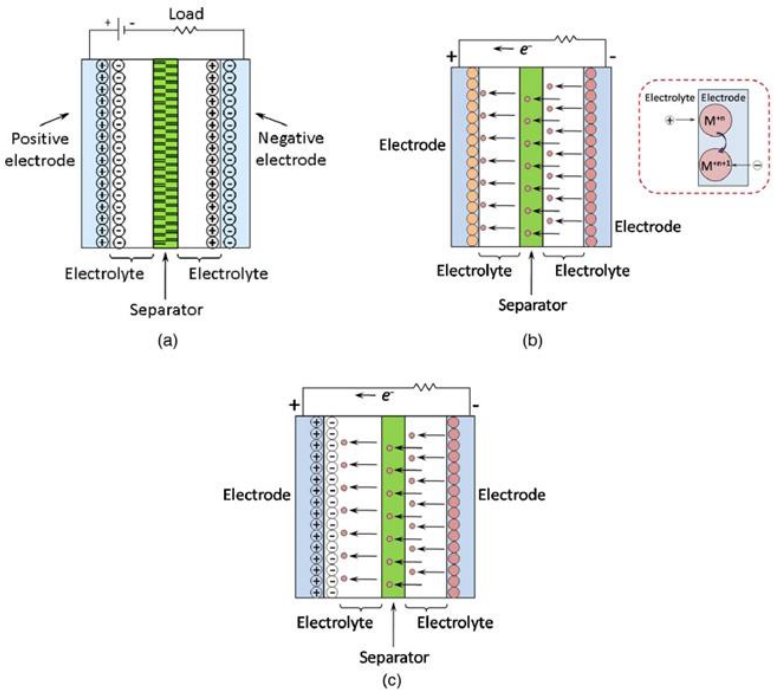

Figure 1.2: Schematic diagram of types of supercapacitor: (a) EDLC (b) pseudocapacitor and (c) hybrid capacitor (Vangari, Pryor, & Jiang, 2013)

The material that generates both EDLC and PC behavior, for instance, redox faradic and non- faradic reaction simultaneously, is known as a hybrid supercapacitor. This type of capacitor is usually constructed by the materials that exhibit both mechanisms, for example, porous carbon materials supported with metal oxide or a conducting polymer**.**

1.2 Fabrication of polymer fibers by electrospinning process

Electrospinning is a standout amongst the most adaptable procedures to produce polymer fibers. Polymer fibers ranging from a few micrometers to nano meters are easily producible by the electrospinning process. Typically, solutions of melted or blended polymers are loaded on a syringe connected to a pump. A high voltage is applied on the needle attached to the syringe which works as a positive electrode. A collector, usually a flat or drum shaped aluminium base acts as a negative electrode. Figure 1.3 A illustrates a basic setup of electrospinning device.

When a drop of polymer solution come out from the tip of the needle, it forms a conical shape recognized as the Taylor cone (Figure 1.3 B) (Yarin, Koombhongse, & Reneker, 2001). Because of the expulsion force between the charged polymer fluid and the remotely associated electric field, a charged plane rises up out of the tip of the Taylor cone precisely at an adequate voltage when the repulsive force of the charged polymer debilitates the surface strain (Z. M. Huang, Zhang, Kotaki, & Ramakrishna, 2003). As the electrically charged jets approach near the lower potential regions, the solvent evaporates and development of the electrostatic force ensues, which causes the charged polymer to further lengthen.

In the event that the connected voltage is not enough high, beads will form from the jet, which is recognized as Rayleigh instability (Reneker & Yarin, 2008).

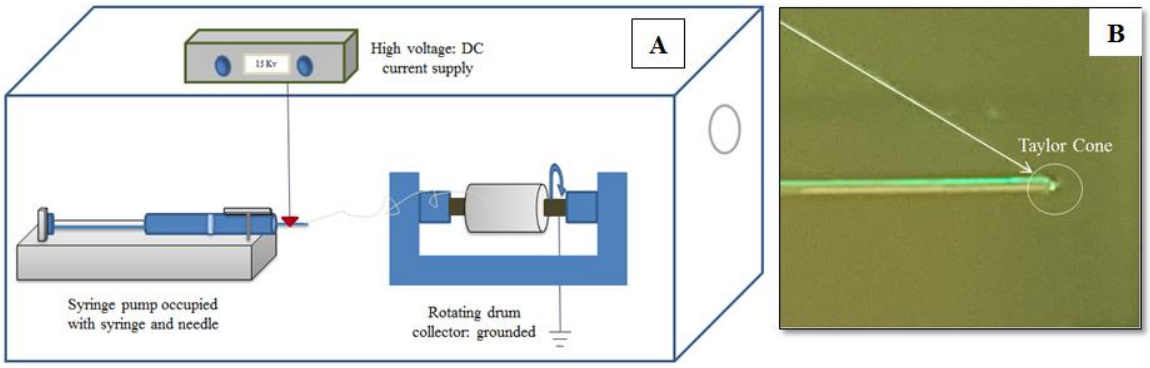

Figure 1.3: (A) schematics of an electrospinning setup; (B) formation of Taylor cone

Electrospun of any polymer which has dissolvable condition at room temperature if its molecular weight is adequately high. The morphology of the fibers enormously relies on the polymer's molecular weight (Inagaki, Yang, & Kang, 2012). It reveals the entanglement of polymer chains in solutions, known as viscosity. The careful consideration of many other operating parameters is the key to creating ultrafine nanofiber ranges. For instance, such operating parameters include voltage applied, solution's flow rate, separation between the spout and grounded collector, environmental factors (e.g. humidity, temperature, velocity of the air in the chamber), and properties of solution (i.e. viscosity, conductivity and surface tension).

1.3 Pyrolysis process

Polymer fibers produced from dissolved PAN solution undergo further modification by pyrolysis processes. Pyrolysis is defined as the decomposition of organic material by a

thermochemical process at certain temperature in the absence of oxygen. It is an irreversible process which simultaneously changes the chemical composition and physical phase of the materials. PAN fibers could be subjected to four pyrolysis processes, among which oxidative stabilization and carbonization are the most essential subjected to convert them into carbon fibers.

1.3.1 Oxidative stabilization

The oxidative stabilization process occurs at a temperature between 180 and 300 ºC under oxygen containing environment at short temperature increment (1 or 2 ºC/min). Prior to high temperature treatment, oxidative stabilization is performed to cross-link PAN chains which stabilize the structure so that it can hold during high temperature treatment (Dalton, Heatley, & Budd, 1999). This process support prevents melting or fusing the fibers in addition to over volatization of elemental carbon during the carbonization hence maximizing the carbon yield from the fibers (J. C. Chen & Harrison, 2002). A complex chemistry occurs on PAN structure during this process, among which the cyclization of the nitrile group (C≡N) and formation of chain structure ($-C=N-C=N-$) due to cross-linking are prominent (G. Zhao, Chen, & Qian, 1992). Figure 1.4 summarizes the proposed reaction mechanism for PAN stabilization process suggested by several studies (Jodeh, 2008).

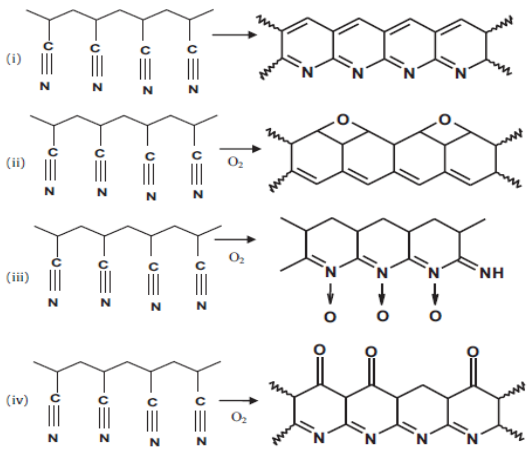

Figure 1.4: Suggested reaction mechanisms for stabilization of PAN homopolymer fiber (Jodeh, 2008)

1.3.2 Carbonization:

After accomplishing the oxidative stabilization stage, carbonization process is applied to convert the polymer fibers into carbon fibers with increased strength (Jodeh, 2008). A remarkable alteration of physical properties and chemical composition occurs in this step (Jing, Wang, Wang, Bai, & Zhu, 2007). The non-carbon elements are eliminated as volatile gases by this process due to high temperature (600-3000 ºC) under inert gas atmosphere, and introduces polymerization and aromatic growth (Rahaman, Ismail, & Mustafa, 2007). Use of a high temperature increment rate is not recommended because it may diffuse the fibers and change their morphology (Jodeh, 2008; Nataraj, Yang, & Aminabhavi, 2012; Wangxi, Jie, & Gang, 2003). A significant change happens due to the heat treatment of PAN based polymer fibers (Rahaman et al., 2007). At room temperature

it has triple bond structure whereas at 450 ^{o}C the structure turns to ladder structure and finally at 750 ^{o}C, the graphitic structure forms.

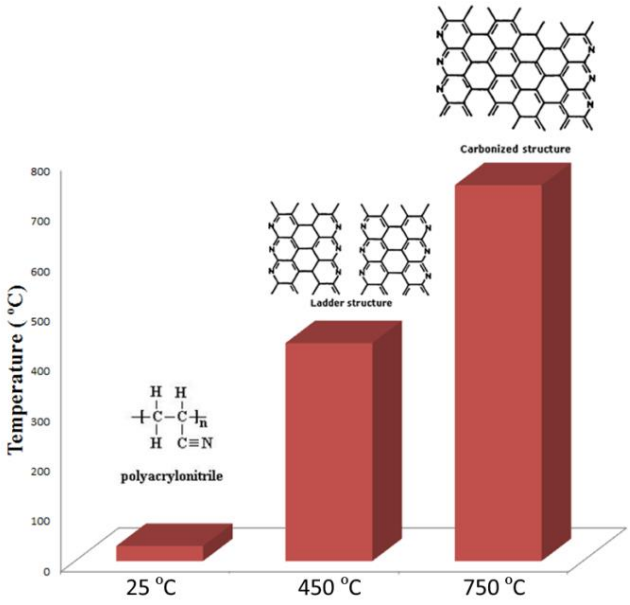

Figure 1.5: Proposed structure of PAN before and after carbonization (Rahaman et al., 2007)

1.4 Co-doping of Nitrogen and Sulfur heteroatoms on carbon materials

The enactment of the supercapacitor can be enhanced by doping of heteroatoms. Heteroatoms are specified as any atoms (Sulfur, Nitrogen, Oxygen, Phosphorous, and Boron) rather than carbon or hydrogen in the skeleton of the molecular structure of the graphite ring. Due to the addition of heteroatoms, chemical properties of the surface improve, which further promotes pseudo-capacitance and wettability of the electrodes by

the formation of a reversible redox reaction (Tian et al., 2015), (B. H. Kim et al., 2013). Hence, the research emphasis has moved to investigating doped-carbon fibers of various heteroatoms as supercapacitor electrode materials. Different sources are being used to acquire these heteroatoms, doping either later or during the fabrication of electrospun fibers, followed by heat treatment and carbonization. The number, sorts, and bonding techniques for heteroatoms on the surface of the carbon materials assumes an imperative part in the physical and chemical properties of the fibers (Zeng et al., 2015).

Nitrogen as a heteroatom in nanostructured carbon materials became a more attractive and well- studied dopant element for SCs because of its superiority to improve electrical conductivity as well as materials availability and low cost (Tian et al., 2015). The electrode materials having hydrophilic and polar nature could likewise be improved because of the existence of the N-group, which further expands the operation of surface area in aqueous electrolyte solutions (Zeng et al., 2015).

Besides nitrogen as heteroatom, sulfur containing carbon materials showed positive behavior towards the enhancement of supercapacitor performance. The electron rich outer shell of the sulfur atom when combined with conjugated carbon, synergistically activates electron density on the surface of the material (Kiciński, Szala, & Bystrzejewski, 2014). Furthermore, S-doped carbon materials generate a series of re-dox faradic reactions (pseudo-capacitive properties) which are rare on pure carbon materials (Xiaochen Zhao et al., 2012).

However, more than one heteroatom such as N and S can be doped on carbon materials. This phenomenon is known as co-doping. The presence of both atoms on the material by carbon structure further improves the transportation of electrons, electrical conductivity in addition to the capacitance value (Tsubota, Takenaka, Murakami, & Ohno, 2011).

1.5 Microwave assisted metal loading on carbon materials

Pristine carbon materials are promising materials to generate EDLC properties on SCs that exhibit long cyclability and high capability rate, however exhibit low specific capacitance (C_S). In addition to heteroatom doping, when metal oxide or hydroxide are presence on carbon material's surface, the C_S double or is enhanced even more than pure carbon materials. Subsequently, an extensive variety of metal oxides has been considered to enhance the capacitive performance of supercapacitors. The greater part of the studies appeared the addition of metal precursors during the preparation of electrospun polymer fibers which were then heat treated to convert into CNFs.

Various techniques, such as conventional hydrothermal (F. Lai, Huang, Miao, & Liu, 2015), magnetic-field (Shao, Li, Zhou, & Hu, 2014) and ultra-sonication assisted (Raj, Ramprasad, Asiri, Wu, & Anandan, 2015) hydrothermal treatment, were employed to load the metal particles on carbon materials. Among these techniques the hydrothermal method assisted with microwave has essential advantages, including extraordinary reaction rate, constant heating of the solution medium, and the possibility to control the phase composition (Egorysheva, Gaitko, Rudnev, Kuvshinova, & Yapryntsev, 2015).

Microwave is a type of electromagnetic radiation which lies among infrared radiation and radio waves in the electromagnetic spectrum (Menéndez et al., 2010). The range of the micro waves ranges between 1 meter to 1 mm and 300 to 0.3 GHz frequency. It is very widely used in telecommunication technology and has very negligible effect on human health. Furthermore, the use of microwave in food heating is widely acceptable and popular method.

The deposition of metal particles on carbon materials by microwave technique is assured because carbon materials are very good absorbents of microwave radiation. So when both metal and carbon material reach equilibrium temperature they come close to each other and combine together.

Chapter 2

2. Literature review

Electrode materials (EMs) assume a key part and involve the vital segment of supercapacitors. EMs of SCs are generally produced using three sorts of materials: porous carbon with high surface territory, oxides/hydroxide/nitrides of different transition metals, and conducting polymers (He et al., 2013). Carbon materials with porous structure, carbon nano tubes (CNT), reduced graphene oxide (RGO) which exhibits EDLC characteristics shows excellent life time cyclability and high power density, but low specific capacitance and poor energy density (He et al., 2013), (Frackowiak & Béguin, 2001). Whereas, transition metal oxide/hydroxides/nitrides, such as MnO_2, SnO_2, CuO, Co_3O_4, RuO_2, TiN, and their binary counterparts are categorized as PCs electrode materials showing relatively high energy density and specific capacitance but poor cyclability and power density (He et al., 2013), (F. Lai et al., 2015). Keeping in mind the end goal (to enhance the overall performance for SCs), a wide range of preparation methods for SC's electrode materials are extensively explored, such as hydrothermal (Hu, Chang, & Wang, 2007; J. Wang et al., 2016), template-assisted method (B. G. Choi, Yang, Hong, Choi, & Huh, 2012; Lo, Jheng, Huang, & Tseng, 2015) chemical vapor deposition (P. Xu et al., 2014), wet spinning (Ma et al., 2016), (Shaohua Chen et al., 2015) and electrospinning (S. Y. Kim, Kim, Yang, & Oshida, 2012; Liu et al., 2015; Y. Xu, Wang, Shen, Dou, & Zhang, 2015). Among many techniques in recent years, electrospinning gained vast interest due to its convenient processability, uniform

dispersity of active materials, operational flexibility, mass productivity and possibility of producing free-standing flexible carbon materials (Al-Enizi et al., 2014; S Chen et al., 2013). Moreover, electrospinning based carbon materials influence the performance of the supercapacitor by improving the specific surface area, surface chemical properties, conductivity, and pore structure with appropriate size and distribution (Zeng et al., 2015), (Bhagwan et al., 2015). Large portions of the late studies exhibited that, electrospun fibers mat followed by stabilization and carbonization, could be utilized directly as electrodes in SCs excluding the polymer binder because of their free-standing and flexibility nature (Z. Zhou & Wu, 2013).

Upon analyzing the articles published from 2012 to 2016 years, it was found that the amount of publications rapidly increased in these 5 years period (Figure 2.1). In 2012, articles related to electrospun based materials for supercapacitor application were 40 whereas this doubled by 2014. In 2015, around 107 articles were published, whereas in 2016, 69 were published within only a 4 months' period. This data reveals that the research on electrospun based materials for supercapacitor applications is increasing very fast.

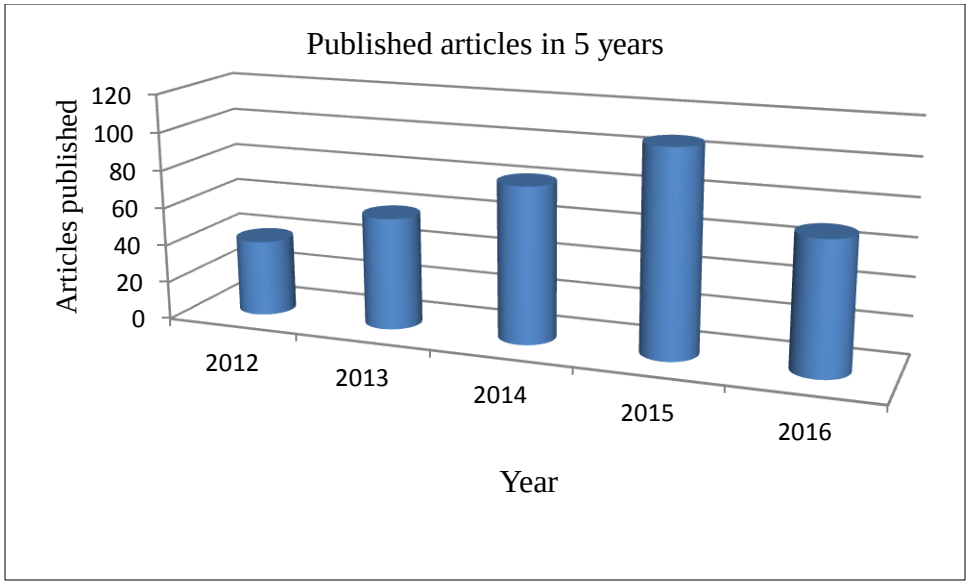

Figure 2.1: Progression of published articles on electrospun based carbon fibers for SC applications in 5 years

2.1 Electrospun carbonaceous materials for supercapacitor applications:

Energy devices with high-performance are required to meet the ever-growing needs and thus SCs are promising constituents. Carbon nanostructured (NS) (T. Chen & Dai, 2013), (Candelaria et al., 2012), (Frackowiak, 2007; Hao, Li, & Zhi, 2013; X. Li & Wei, 2013; Niu, Zhang, Xie, Wang, & Lin, 2011; Pandolfo & Hollenkamp, 2006; Staaf, Lundgren, & Enoksson, 2014; L. L. Zhang, Zhou, & Zhao, 2009) graphene NS (H. J. Choi et al., 2012), (W. Yang et al., 2015) and hybrid NS (van Schalkwijk W., 2005; G. Yu, Xie, Pan, Bao, & Cui, 2013; Z. Yu, Tetard, Zhai, & Thomas, 2015) materials are widely presented along with their synthesis methods, characteristics, various performance measures and applications for energy related applications, more specifically for SCs applications (A.

Yu et al., 2015), (Vangari et al., 2013). However, the utilization of electrospinning technique in the production of carbonaceous materials for energy related application is not being overlooked (Niu et al., 2011), (Inagaki et al., 2012; Mao, Alan Hatton, & Rutledge, 2013; Ra, Raymundo-Piñero, Lee, & Béguin, 2009; Shi et al., 2015; B. Zhang, Kang, Tarascon, & Kim, 2015; L. Zhang, Aboagye, Kelkar, Lai, & Fong, 2014). Figure 2.2 demonstrates carbon fibers created by electrospinning took after by stabilization and carbonization.

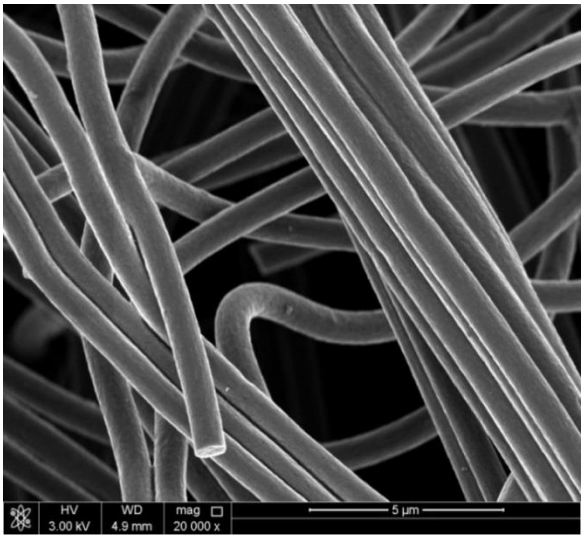

Figure 2.2: SEM micrograph of electrospun based carbon nano fibers

Among energy storage devices, SCs gained more attention due to their promising trend as next generation energy storage. Figure 2.3 shows discussed performance of materials for SCs application by electrospinning technique.

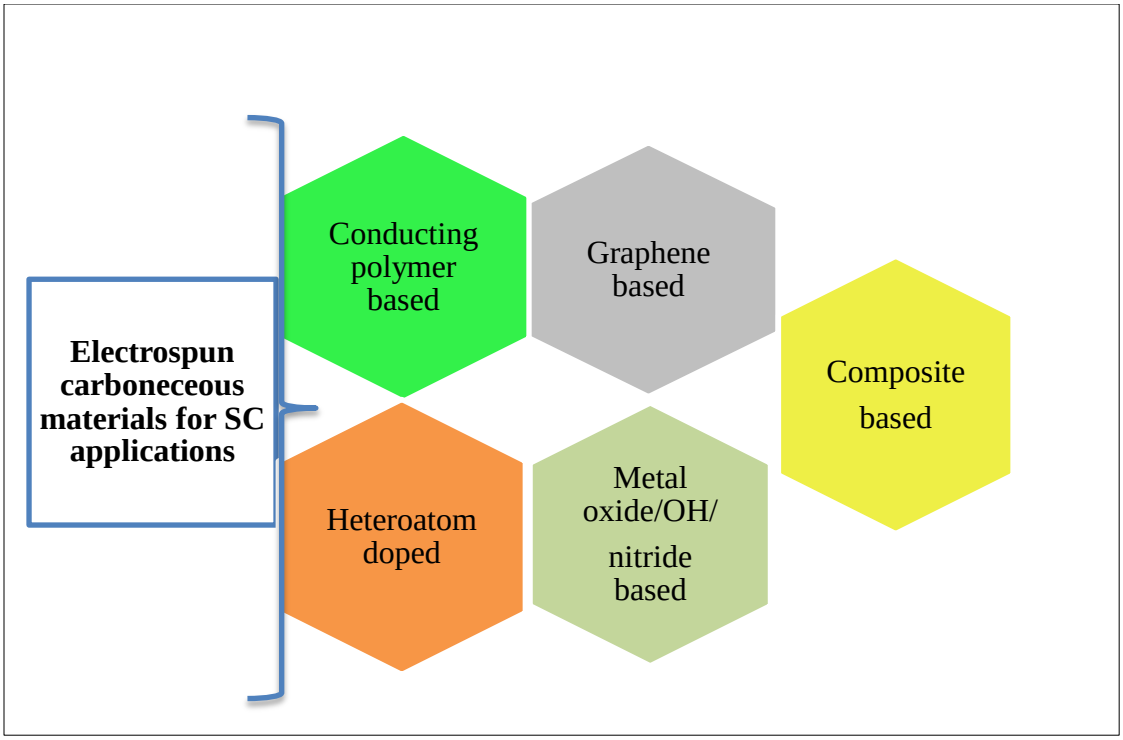

Figure 2.3: Discussed electrospun carbonaceous materials for SC application

2.2 Heteroatom doped electrospun nanofibers for SC application:

The performance of the supercapacitor could be improved by doping of heteroatoms. Heteroatoms are specified as any atoms (S, N, O, P, B) rather than carbon or hydrogen in the skeleton of the molecular structure of the graphite ring. With the addition of heteroatoms, chemical properties of the surface improve, which further promotes pseudo-capacitance and wettability of the electrodes by the formation of reversible redox reactions (Tian et al., 2015), (B. H. Kim et al., 2013). Hence, the research emphasis has promoted investigation of doped-carbon fibers of various heteroatoms as supercapacitor electrode materials. Different sources are being used to acquire these heteroatoms, doping

either later or during the fabrication of electrospun fibers, followed by heat treatment and carbonization. The types, number, and bonding methods of heteroatoms on the surface of the carbon materials plays a vital role on the physical and chemical properties (Zeng et al., 2015).

Nitrogen as heteroatom in nanostructured carbon materials became a more attractive and well- studied dopant element for SCs because of its superiority to improve electrical conductivity as well as materials availability and low cost (Tian et al., 2015). Moreover, the hydrophilic and polar nature of the electrode materials could also be enhanced due to the presence of N-group which further expands the operation of surface area in fluid electrolyte solutions, (Zeng et al., 2015). Tian et al. has achieved highest C_S of 251.2 $F.g^{-1}$ for their N-enriched porous CNF materials which showed specific surface area (SSA) of 736 $m^2 g^{-1}$ (Tian et al., 2015). They demonstrated that post-treatment, such as treating carbon material with ammonia rather than employing N sources on precursor preparation, led to the rich N content of 5.26 at. % on the synthesized materials. Furthermore, Huang et al. attained SSA of 656 $m^2 g^{-1}$ and N content of 8.1 at.% for their PAN/ PEG-PSO-PEG blend where PAN acts as the precursor of N-doped carbon and PEG-PSO-PEG forms the mesopores on the material (K. Huang, Yao, Yang, Chen, & Li, 2016). They claimed that, the C_S of 289 $F.g^{-1}$ was accomplished as a consequence of high SSA, improved wettability, formation of macroporous, mesoporous, graphenic structure and quaternary nitrogen source. A high SSA of 1125.53 $m^2 g^{-1}$ was achieved by Zeng et al. for CNF produced from PAN-PMMA/TEOS precursors blend (Zeng et al., 2015). Large SSA, high volume of pores and hierarchical pore size distribution resulted in a C_S of 207 $F.g^{-1}$.

Xu et al. fabricated N-doped hollow CNF with N content of 8.2 at.%. Their synthesized material exhibited SSA of 701 $m^2 g^{-1}$ and C_S of 197 $F.g^{-1}$ due to the formation of a hollow structure and a high level of N-doping (Q. Xu et al., 2015).

Rather than mono heteroatom, binary sources of heteroatoms are also investigated by many groups. Wei et al. recently studied N and O doped ultrafine CNFs as flexible electrode material for SC (Wei et al., 2016). C_S of 86 $F.g^{-1}$ was achieved with PAN: PMMA mixing ratio of 3:7. They claimed that high SSA, interconnected micro/ meso/ macro pore formation, and presence of quaternary and pyridinic-N oxides attributed to the obtainable C_S value. Furthermore, Kim et al. prepared Boron (B)- Nitrogen (N) doped CNF where, H_3BO_3 and Urea act as the source of B and N respectively. A high concentration level of B:N=20:4 resulted in the highest C_S of 180 $F.g^{-1}$ and SSA of 559 $m^2 g^{-1}$ due to the porous structure and pseudo-capacitive effect (B. H. Kim et al., 2013). Table 2.1 shows the summary of (i) materials and BET surface area (ii) specific capacitance, (iii) proposed reason of specific capacitance performance.

Table 2.1: Summary of performance of Heteroatom doped CNF

i) Materials	**ii) Specific Capacitance ($F.g^{-1}$) at scan rate ($A.g^{-1}$)**	**iii) Proposed reason for the SC performance**	**Ref.**
N-enriched porous CNF S_{BET} = 763 m^2/g	251.2 F. g^{-1} at 0.1 $A.g^{-1}$	high SSA, profuse nitrogen and oxygen functional groups, and electrical conductivity	(Tian et al., 2015)
Hierarchical porous N-doped CNF S_{BET} = 656 m^2/g	289 $F.g^{-1}$ at 0.2 $A.g^{-1}$	high SSA, improved wettability, formation of macroporous, mesoporous and graphenic structure and quaternary nitrogen source	(K. Huang et al., 2016)
N-doped hollow activated CNF S_{BET} = 701 m^2/g	197 $F.g^{-1}$ at 0.2 $A.g^{-1}$	formation of hollow structure and high N-doping level	(Q. Xu et al., 2015)
Nitrogenous hierarchical porous CNF S_{BET} = 1125.53 m^2/g	207 $F.g^{-1}$ at 0.2 $A.g^{-1}$	substantial BET surface range, high pore volume and various leveled pore size distribution	(Zeng et al., 2015)
N, O doped-ultrafine CNFs S_{BET} = 467 m^2/g	86 $F.g^{-1}$ at 5 mVs^{-1}	high SSA, interconnected micro/ meso/ macro pores formation and presence of quaternary and pyridinic-N oxides	(Wei et al., 2016)
Boron-Nitrogen@CNF S_{BET} = 559 m^2/g	180 $F.g^{-1}$ at 1mA cm^{-2}	porous structure and pseudo-capacitive behavior	(B. H. Kim et al., 2013)

2.3 Metal oxide activated electrospun nanofibers for SC application

Activation of CNF by nanostructured transition metal oxide (MOs)/hydroxide became very attractive typical electrode material for Pseudo capacitors owing to their favorable redox potential and conductivity to store electrical charge, compatible interaction with polymer fibers, and capability to improve porosity of CNF in addition to high C_S performance (Kumar, Subramania, & Balakrishnan, 2014). In this regards, numerous sources of mono, binary and ternary metal oxides/OH/nitrides such as Co_3O_4, CuO, Fe-CeO_2, Mn_xO_x, MnO_x-SnO_2, NiO, Ni-Co, RuO_2, Sr-Ln-Ni, TiO_2, V_2O_5, VN are presented as high performance supercapacitor materials.

Vidyadharan et al. synthesized Co_3O_4 nanowire from PVA/CoAc blended solution using electrospinning followed by stabilization and heat treatment (Vidyadharan et al., 2014). A high C_S of 1110 $F.g^{-1}$ was reached at a current density of 1 $A.g^{-1}$ as a result of highly fractioned electrochemically active surface and high theoretical capacitance of cobalt oxide. Furthermore, Kumar et al. reported a C_S of 407 $F.g^{-1}$ at a scan rate of 5 mVs^{-1} for their Co_3O_4 nanofibers produced from PVP/CoAc blend (Kumar et al., 2014). They claimed that facile electrolyte penetration and well utilization of electro-active surface are the reason of this high C_S value.

CuO nanowire as anode material for SC has been constructed for the first time by Vidyadharan et al. (Vidyadharan, Misnon, Ismail, Yusoff, & Jose, 2015). Using commercial carbon electrode as cathode they reached C_S of 83 $F.g^{-1}$ and larger voltage window of (V ~1.6 V) for asymmetric supercapacitor (ASC). They suggested that the exhibited ASC could be marketed inferable from the more noteworthy plenitude of

copper in the world's covering and positive charge storage properties of their material. Moreover, a binary metal oxide activated CNF was synthesized through FeAc/CeAc/PVA blend by Ghouri et al (Ghouri, Barakat, Alam, Park, & Han, 2015). A C_S of 83 $F.g^{-1}$ was achieved owing to the nature of catalyst and support material as well as crystal size and attributed morphology.

Among other metal oxides, Mn_xO_x based CNF materials gained additional attention as PC electrode materials because of their high theoretical specific capacitance (~1110 $F.g^{-1}$) in aqueous electrolyte, natural abundance, cost effectiveness, eco-friendliness and wide potential windows (D. Zhou et al., 2015). Wide structural varieties of Mn_xO_x based CNF, such as MnO_2 nanoflakes (D. Zhou et al., 2015), 3D MnO_x (Lee, Lee, & Kim, 2014), Porous 1D Mn_3O_4 nanofibers (Bhagwan et al., 2015), MnO_x nanocrystals (Xin Zhao, Du, Li, & Zhang, 2015), MnO_x/SnO_2 hybrid CNF (Mondal, Tsai, Stout, & Talapatra, 2015) and AAC/MnO_2 nanoflakes (Zhi, Manivannan, Meng, & Wu, 2012), has been proposed by different groups which showed a relatively high C_S performance. Table 2.2 outlines the (i) materials (iii) specific capacitance, (iii) proposed reason of C_S performance for different transition metal based CNF materials that are Mn_xO_x based.

Table 2.2: Summary of performance of activated CNF by metal oxide doped CNF

i) Materials	iii) Specific Capacitance ($F.g^{-1}$) at current density ($A.g^{-1}$)	iv) Proposed reason for the C_S performance	Ref.
Co_3O_4 nanowire S_{BET} = 13.6 m^2/g	1110 $F.g^{-1}$ at 1 $A.g^{-1}$	high fraction of electrochemically active surface and high theoretical capacitance of cobalt oxide	(Vidyadharan et al., 2014)
Co_3O_4@CNF S_{BET} = 67 m^2/g	407 $F.g^{-1}$ at 5 mVs^{-1}	facile electrolyte penetration and better utilization of electroactive surface	(Kumar et al., 2014)
CuO nanowire	83 $F.g^{-1}$ at 2 $A.g^{-1}$	higher electrical conductivity of the nanowires electrode with high crystallinity	(Vidyadharan et al., 2015)
Fe/CeO_2@CNF	83 $F.g^{-1}$	nature of catalyst and support material, crystal size and morphology	(Ghouri et al., 2015)
MnO_2 nanoflakes	520 $F.g^{-1}$ at 0.5 $A.g^{-1}$	intriguing structural features	(D. Zhou et al., 2015)
3D MnO_x@CNF	360.7 $F.g^{-1}$ at 1 $A.g^{-1}$	unique 3D morphology coupled with a reduced charge transfer resistance of the mixed phase of Mn_2O_3 and Mn_3O_4	(Lee et al., 2014)
Porous 1D Mn_3O_4 nanofiber S_{BET} = 24 m^2/g	210 (±5) $F.g^{-1}$ at 0.3 $A.g^{-1}$	unique nanofibric morphology, 1D and high aspect ratio nanofibers	(Bhagwan et al., 2015)
MnO_x nanocrystals	174.8 F. g^{-1} at 2 mVs^{-1}	Enhanced conductivity and net-like CNFs backbones	(Xin Zhao et al., 2015)
MnO_x/SnO_2 hybrid CNF	472.31 F. g^{-1} at 10 mVS^{-1}	High conductivity of SnO_2 created path for electrons transportation that acts as channels for ions from electrolyte	(Mondal et al., 2015)
AAI-CNF/MnO_2	311 F. g^{-1} at 2 mVs^{-1}.	High specific surface area of CNF and enhanced electronic conductivity	(Zhi et al., 2012)

Among numerous MOs, Nickle oxide (NiO) is especially appealing because of its high hypothetical capacitance (2573 $F.g^{-1}$), great thermal and chemical stability, earth-plenitude and natural amicability (Kundu & Liu, 2015). Moreover, binary metal

hydroxides such as Ni-Co showed high redox activity and improved electrical conductivity (F. Lai et al., 2015). Vidhyadharan et al. fabricated NiO nanowires by electrospinning an aqueous polymeric solution comprising nickel precursor followed by heat treatment and carbonization (Vidhyadharan et al., 2014). They ensured that, due to high degree of crystallinity and lower diameter of NiO nanowires a significant specific capacitance of C_S 670 $F.g^{-1}$ at 1 $A.g^{-1}$ was achieved. Kundu et al. fabricated porous NiO CNF on Ni foam which exhibited C_S of 737 $F.g^{-1}$ at 2 $A.g^{-1}$ ascribed to the permeable nature of both NiO-NFs and the Ni foam and binder-free property of the electrode (Kundu & Liu, 2015). Furthermore, an excellent C_S performance of 1378.2 $F.g^{-1}$ and 1195.4 $F.g^{-1}$ at current density of 1 $A.g^{-1}$ was achieved for Ni/Co nanorods and Ni/Co nanowires correspondingly (F. Lai et al., 2015). Lai et al. claimed that, fully exposed active sites of the synthesized materials and improved specific surface area are the reason of this high performance (F. Lai et al., 2015). It is worth mentioning that the effect of temperature could dominate the electrochemical capacitive property of synthesized materials. Lai et al. fabricated $Ni(OH)_2$/CNF material and investigated temperature effect through annealing at different temperatures (C.-C. Lai & Lo, 2015). They found that the material annealed at 300 ºC showed higher capacitance value of 455.0 C/g at scan rate of 2 mV/s owing to the cooperative performance of conducting linkages provided by CNFs and the existence of faradaic reactions of $Ni(OH)_2$ nanoflakes. Table 2.3 summarizes the proposed reason of C_S performance for various NiO/$Ni(OH)_2$ based CNF materials for SCs application.

Table 2.3: Summary of performance of activated CNF by $NiO/Ni(OH)_2/CNF$

i) Materials	**iii) Specific Capacitance ($F.g^{-1}$) at current density ($A.g^{-1}$)**	**iv) Proposed reason for the C_S performance**	**Ref.**
Porous NIO-NFs	737 $F.g^{-1}$ at 2 $A.g^{-1}$	porous nature of both NiO-NFs and the Ni foam, binder-free electrode	(Kundu & Liu, 2015)
NiO@CNF S_{BET} = 14 m^2/g	670 $F.g^{-1}$ at 1 $A.g^{-1}$	lower diameter and high degree of crystallinity of NiO nanowires	(Vidhyadharan et al., 2014)
Ni/Co nanorods and Ni/Co nanosheets	1378.2 and 1195.4 $F.g^{-1}$ at 1 $A.g^{-1}$	improved SSA and fully exposed active sites	(F. Lai et al., 2015)
$Ni(OH)_2$ nano-flakes@CNF-300°C S_{BET} = 49 m^2/g	455.0 C/g at scan rate of 2 mV/s	cooperative performance of conducting linkages provided by CNFs and the existence of faradaic reactions of $Ni(OH)_2$ nanoflakes	(C.-C. Lai & Lo, 2015)

Table 2.4 outlines the (i) materials (ii) specific capacitance(CS) and (iii) proposed reason of CS performance for different transition metal based CNF materials for SCs application.

Table 2.4: Summary of performance of activated MOs/$M(OH)_2$/MN doped CNF

i) Materials	**ii) Specific Capacitance ($F.g^{-1}$) at current density ($A.g^{-1}$)**	**iii) Proposed reason for the C_S performance**	**Ref.**
TiC/C@CNF S_{BET} = 340.1 m^2/g	130 $F.g^{-1}$ at 0.1 $A.g^{-1}$	synergistic effect between TiC and carbon	(Ren, Dai, Pang, Liu, & Yu, 2015)
1D VN@CNF	291.5 F. g^{-1} at 0.5 $A.g^{-1}$	rapid transport for charge and ion, additional active sites for both adsorption and faradic reaction of nanoparticles embodied into carbon materials	(Y. Xu et al., 2015)
RuO_2@CNF	188 $F.g^{-1}$ at 1 $mAcm^{-2}$	large mesopores induced by PMMA and RuO_2 in CNF	(B.-H. Kim, Kim, & Lee, 2016)
TiC-CDC nano-felts-1000ºC S_{BET} = 1188 m^2/g	135 $F.g^{-1}$	microstructure of the TiC-CDC nano-felts; i.e., the disarranged and exceedingly permeable carbon coinciding with graphitic carbon strips in the nanofiber network	(Gao et al., 2012)
V_2O_5@CNF S_{BET} = 595.21 m^2/g	150 $F.g^{-1}$ at 25 mV s^{-1}	larger interfacial area between the carbon and V_2O_5 domains	(B.-H. Kim, Kim, Yang, Rahy, & Yang, 2012)
HybTi@CNFs S_{BET} = 697 m^2/g	280.3 $F.g^{-1}$ at 1 $A.g^{-1}$	unique integrated crystal and amorphous structure	(Tang et al., 2016)
TiO_2@CNF	310 $F.g^{-1}$	synergic effect of PC of TiO_2 nanofibers and EDLC of activated carbon	(Kolathodi & Natarajan, 2015)
$La_xSr_{1-x}NiO_{3-\delta}$ @CNF S_{BET}= 15.462 m^2/g	719 $F.g^{-1}$ at 2 $A.g^{-1}$	Formation of perovskite structure	(Cao, Lin, Sun, Yang, & Zhang, 2015)

2.4 Conducting polymer based electrospun nanofibers for SC applications:

Beside heteroatom and metal oxide based CNF materials, conducting polymer (CPs) supported carbon materials became very popular as SC electrode material because of their high particular surface range, oxidation/reduction behavior, controllable electrical conductivity, easy to process, inexpensiveness and higher environmental stability (J. E. Yang et al., 2013). For instance, polyaniline (PANI), polythiophene (PTh) and polypyrrole (PPy) are the most common types of CPs considered as promising electrode materials for pseudocapacitors (PCs). Many groups have developed high performance PC electrode materials by employing CPs. Yang et al. fabricated vine-like nanostructured PANI by electrochemically polymerization on activated carbon nanofibers (ACNFs) (J. E. Yang et al., 2013). Pristine CNF reached SSA of 1200 m^2/g after activation, upon which the PANI were polymerized, resulting a C_S of 832 $F.g^{-1}$ at 1 $A.g^{-1}$ attributed to the synergic effect of an electrical double-layer formed by ACNF and oxidation-reduction behavior of PANI nanostructure. Miao et al. demonstrated in-situ polymerization of PANI on CNF resulting in PAN-PANI core shell arrangement (Miao et al., 2015). They asserted that, owing to their synthetic impact of unique structural characteristics, a C_S of 577 $F.g^{-1}$ at a scan rate of 5 mV/s has achieved. He et al. fabricated PANI nanowhiskers wrapped on graphitized electrospun CNF (GENFs) (He et al., 2013). They stated that, due to high electrical conductivity of GENFs network (5.4 S cm^{-1}) and 3D interconnected frameworks with a macroporous architecture a C_S of 176.5 $F.g^{-1}$ at 0.5 $A.g^{-1}$ has achieved.

Table 2.5 outlines the (i) materials (ii) specific capacitance and (iii) proposed reason of specific capacitance performance for conducting polymer based CNF materials.

Table 2.5: Summary of conducting polymer doped CNF materials

i) Materials	**ii) Specific Capacitance ($F.g^{-1}$) at current density ($A.g^{-1}$)**	**iii) Proposed reason for the C_S performance**	**Ref.**
PANI-ACNF	832 $F.g^{-1}$ at 1 $A.g^{-1}$	synergic effect of electric double-layer of ACNF and redox reaction of PANI nanostructure	(J. E. Yang et al., 2013)
PAN@PANI	577 $F.g^{-1}$ at 5 mV/s	synthetic impact of their unique structural characteristics	(Miao et al., 2015)
PPy@CNFs	236 $F.g^{-1}$ at 1 mVs^{-1}	High SS, porosity, good electrical conductivity with enormous active sites	(Cai et al., 2015)
PANI@CNFs	407 at 5 mV/s	High mass loading and uniform formation of PANI	(Miao et al., 2016)
3D nanowhiskers	176.5 F. g^{-1} at 0.5 $A.g^{-1}$	high electrical conductivity of GENFs network (5.4 S cm^{-1}) and 3D interconnected frameworks with a macroporous architecture	(He et al., 2013)
Porous N-doped CNFs@PPy S_{BET} = 348.12 m^2/g	202.0 F. g^{-1} at 1.0 $A.g^{-1}$	"combined effect of a high N-doping level changing the electron donor/acceptor characteristics of carbon and a large BET surface area increasing the surface area accessible for electrolyte ion transport"	(Li-feng Chen et al., 2012)
Cross-linked N-doped CNF	175 $F.g^{-1}$ at 50 $A.g^{-1}$	Formation of more access sites for electron transfer in the network	(Cheng et al., 2015)

2.5 Graphene based electrospun nanofibers for SC applications:

Since the last decade, graphene based materials has drawn extensive consideration as an electrode material for electrochemical supercapacitors. Graphene, which is a 2 dimensional (2D) carbon lattice with honeycomb structure comprises monolayered or multilayered graphitic nanosheets (Shaohua Chen et al., 2015). Distinct forms for instance graphene oxide (GO) and reduced graphene oxide (RGO) have also been introduced (Hsu et al., 2015). These materials exhibit novel properties, including relatively high surface area, sufficient porosity, extremely high mechanical stiffness, exceptional electrical conductivity, superior chemical stability, extensive surface chemistry, high aspect ratio, broad electrochemical window, flexibility, and comparably inexpensive fabrication process (Hsu et al., 2015; Liu et al., 2015; Y. Wang et al., 2014; W. Yang et al., 2015). A wide variety of impressive research showed, composite or hybrid structure of graphene based materials enhance electrical and mechanical properties for the host materials.

Liu et al. fabricated N-doped RGO-CNF composites, where they used nitrogen or ammonia gas as the source of nitrogen during carbonization (Liu et al., 2015). Although they introduced the materials for capacitive deionization application, it exhibited a high C_S of 337.85 F. g^{-1} ascribed to n-type heteroatom(N) doping, and thereby creating an active "plane-to-line" conducting network. Wang et al. produced flexible SC material by electrospun polyamide-66 fabric incorporation reinforced RGO nanosheets by deep coating followed by heat treatment (Y. Wang et al., 2014). They demonstrated 3 different sized nanosheeets, among which medium sized showed expectant C_S of 279.82 F. g^{-1} due

to captivated largest mass of RGO on the CNF, which further facilitated completion of a conductive path. A C_S of 263.7 $F.g^{-1}$ at 0.1 $A.g^{-1}$ was reached for graphene beaded CNF attributed to high electrical conductivity, unique nano-structural configuration and large specific surface area of the fabricated material (Z. Zhou & Wu, 2013). Table 2.6 summarizes the performance of graphene based CNF for SC applications.

Table 2.6: Summary of graphene based CNF for SC applications

Materials	**Specific Capacitance ($F.g^{-1}$) at scan rate ($A.g^{-1}$)**	**Proposed reason for the SSC performance**	**Ref.**
N-doped, RGO-CNF S_{BET} = 864.10 m^2/g	337.85 F. g^{-1}	nitrogen doping and the formation of an active "plane-to-line" conducting network	(Liu et al., 2015)
M-RGO/ PA66-nano	279.82 $F.g^{-1}$	largest mass of M-RGO loading and completed conductive path	(Y. Wang et al., 2014)
Graphene-beaded CNF	263.7 F. g^{-1} at 0.1 $A.g^{-1}$	high electrical conductivity, unique nano-structural configuration and large specific surface area of the graphene nanosheets	(Z. Zhou & Wu, 2013)
CNF/GNS composites S_{BET} = 447 m^2/g	197 $F.g^{-1}$ at 1.25 $A.g^{-1}$	high SSA, small pore size and high conductivity	(Tai, Yan, Lang, & Xue, 2012)
CNF/G composite S_{BET} = 480 m^2/g	183 $F.g^{-1}$ at 1.0 $A.g^{-1}$	unique structure and the synergic effect of graphene and CNFs	(Dong et al., 2013)
GO/CNT@CNF S_{BET} = 175.1 m^2/g	120.5 F. g^{-1} at 0.5 $A.g^{-1}$	enhanced capacitance, electrical conductivity, and formation of network structure.	(Hsu et al., 2015)

2.6 Electrospun Composite nanofibers for supercapacitor application

Research enthusiasm is not yet over for fabricating sole materials like conducting polymer, heteroatom doping, and graphene based materials through electrospinning for SC application. Further interest has been observed on composite/hybrid materials for better performance. Conducting polymer, such as PANI, shows significant specific capacitance of 750 $F.g^{-1}$ but poor cyclability and electrical conductivity while graphene based materials exhibit relatively low $C_{S,}$ but good conductivity and cyclability (Z. Zhou & Wu, 2014). Hence, a combination of both materials might be the optimized circumstance where electrospinning is the medium to construct the bridge.

Zhou et al. demonstrated graphene-beaded CNF surface-coated with nanostructured PANI which showed C_S of 637 $F.g^{-1}$ at 0.15 $A.g^{-1}$ due to the unique microstructures of the heterogeneous G/CNFs coated with ultrathin layers of thorn-like PANI nanorods (Z. Zhou & Wu, 2014). El-Enizi et al. supplemented $NiO/Ni(OH)_2$ on CNF incorporated GO and PANI (Al-Enizi et al., 2014). They studied the effect of calcination temperature on synthesized materials among which, the 400 ºC calcined sample showed high C_S of 738 $F.g^{-1}$ attributed to the morphology of the proposed materials. Table 2.7 summarizes the performance of composite based CNF materials for SC applications

Table 2.7: Summary of composite based CNF materials for SC applications

i) Materials	**ii) Specific Capacitance ($F.g^{-1}$) at Current density ($A.g^{-1}$)**	**iii) Proposed reason for the SSC performance**	**Ref.**
PANI-G/CNFs	637 $F.g^{-1}$ at 0.15 $A.g^{-1}$	novel microstructures of the heterogeneous G/CNFs coated ultrathin layers of thorn-like PANI nanorods	(Z. Zhou & Wu, 2014)
PANI/GO/CNFs-NiO/Ni(OH)$_2$	738 $F.g^{-1}$ at 50 mV s^{-1}	formation of NiO and attributed morphology	(Al-Enizi et al., 2014)
CNFC(TEOS-PAN-Graphene) S_{BET} = 437.64 m^2/g	144.80 F. g^{-1} at scan rate of 25 mV s^{-1}	modified morphological structure, increased SSA and electrical conductivity	(S. Y. Kim et al., 2012)
GO-V_2O_5/CNFs	453.824 F. g^{-1} at scan rate of 10 mVs^{-1}	electrical conductivity and high surface area of graphene oxide	(Thangappan et al., 2014)

Chapter 3

3. Synthesis of supercapacitor electrode materials: Experimental work

The synthesis of electrode materials for supercapacitor application was performed in several steps. The preparation of the materials began with electrospinning polymer fiber, followed by stabilization and carbonization, and ended with metal loading by microwave technique. Figure 3.1 demonstrates the graphical abstracts of complete preparation process.

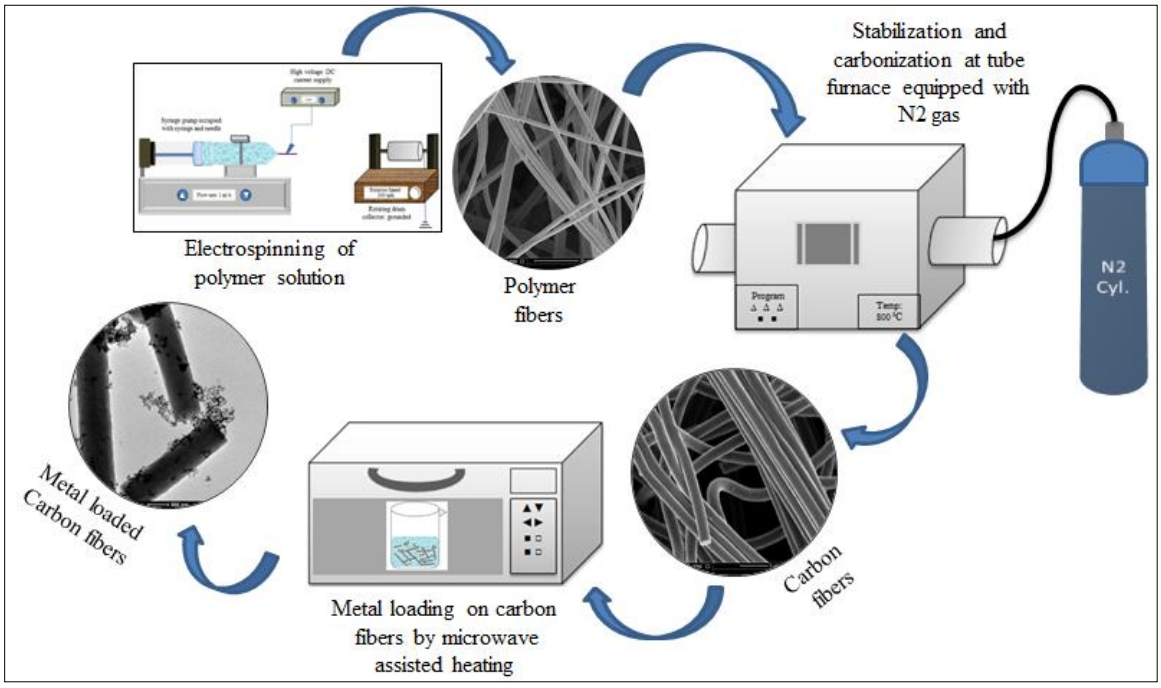

Figure 3.1: Graphical abstract of complete preparation process

3.1Experimental

3.1.1 Materials

Polyacrylonitrile (SIGMA ALDRICH, Average Mw. 150,000); N, N-Dimethylformamide (SIGMA ALDRICH, Assay 99%); Thiourea (Riedel-de Haën, Assay 99%); Ruthenium(III) chloride hydrate (SIGMA ALDRICH); Tin (II) chloride dehydrate (SIGMA ALDRICH); Hydrazine hydrate solution (Fluka); Ethanol (SIGMA ALDRICH; Assay 96%) reagents were used without any further purification. Double distilled water was used throughout the experiments.

3.1.2 Characterization

Four main types of characterizations were carried out throughout the research work to characterize and analyze the properties of prepared materials.

Microscopy

Morphological characterization of the materials was carried out by field emission scanning electron microscope (FE-SEM) and transmission electron microscope (TEM). Figure 3.2 and Figure 3.3 shows SEM instrument (model: FEI NOVA NANOSEM 450) equipped with EDX(Energy-dispersive X-ray) and TEM instrument (model: Tecnai G2-F20 S-TWIN) respectively.

Figure 3.2: SEM instrument model: FEI NOVA NANOSEM 450

Figure 3.3: TEM instrument model: Tecnai G2-F20 S-TWIN

The structural characteristics such as shape, pattern and morphology of materials could be investigating by SEM and TEM. A focused beam of electron interacts with the sample which produces different signals and then generates a morphological structure of the sample's surface and arrangement. Difference between each sample indicate the identification of each material. The magnification of SEM, ranges from micrometer to nanometer level. Whereas, TEM can examine as small as a single column atom.

Spectroscopy

X-ray diffraction (XRD) is a robust procedure used to remarkably distinguish the crystalline stages present in materials and to quantify the basic properties (grain size, imperfection structure, diffraction angle, phase purity and composition) of these phases. XRD is additionally used to decide the thickness of thin films and multi-layers, and nuclear plans in formless materials (polymers) and at interfaces. Figure 3.4 shows XRD instrument model: Rigaku MiniFlex II.

Figure 3.4: XRD instrument model: Rigaku MiniFlex II

X-ray photoelectron spectroscopy model: Kratos AXIS Ultra DLD equipped with monochromatic and dual Al-Mg X-ray source has been used to quantify the elemental composition of materials and identify the binding energies. XPS is one of the most powerful spectroscopy analyzer that quantitatively examine the elemental composition at the parts per thousand range. In addition, the chemical and electronic state of the elements present within the material can also be identified with this technique. The oxidation state and surface chemical bonding's of material are significantly analyzing by this tool. Figure 3.5 shows X-ray photoelectron spectroscopy model: Kratos AXIS Ultra DLD.

Figure 3.5: X-ray photoelectron spectroscopy model: Kratos AXIS Ultra DLD

Structural analysis

Fourier transmittance infrared(FTIR) was used to obtain the vibration frequencies between the bonds of the atoms and to differentiate between the modifications of materials. Figure 3.6 shows FTIR instrument model: PerkinElmer Frontier.

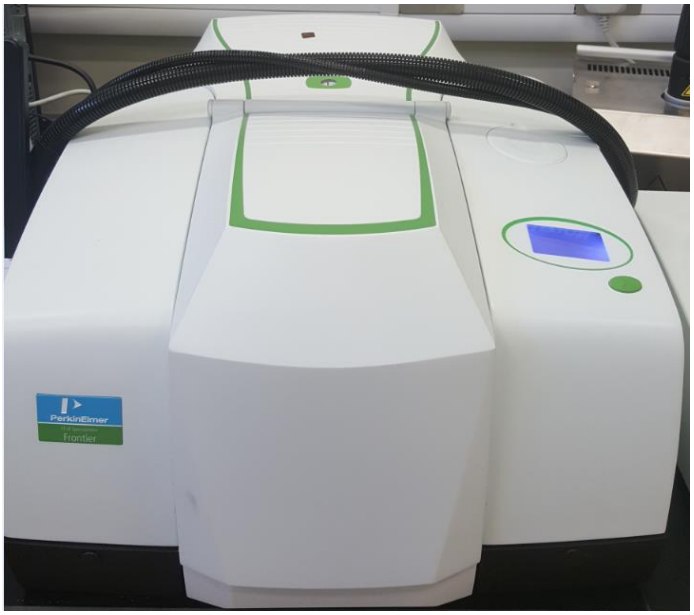

Figure 3.6: FTIR instrument model: PerkinElmer Frontier

Electrochemical analysis

The electrochemical test is one of the most important techniques to determine the performance of supercapacitors at laboratory scale. It is an easy and qualitative technique to measure the performance of prepared materials. The obtained result from cyclic voltammetry is then used to apply on a given equation to calculate the specific capacitance of the materials. Power station instrument model: GAMRY "Reference 600" was occupied to measure the electrochemical performance of the materials. Figure 3.7 shows power station instrument model: GAMRY "Reference 600".

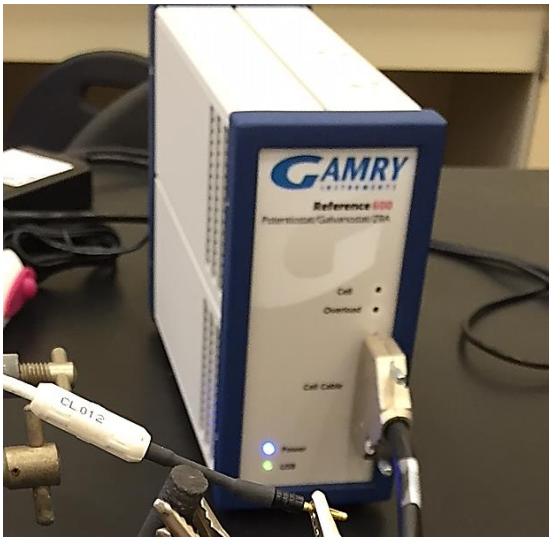

Figure 3.7: Power station instrument model: GAMRY “Reference 600”

3.2 Optimization of fiber formation:

Electrospinning is a crucial technique to optimize the polymer fiber formation because it depends on various parameters (i.e. flow rate, viscosity, high voltage, diameter of needle’s hole). Improper setting up of any parameter may produce beaded fibers, fibers with drops, broken fibers, etc.

To optimize the proper condition of the fibers of Polyacrylonitrile (PAN), we experimented with various circumstances. When PAN was taken weight proportional to volume ratio, the fibers were not properly formed and resulted in block of the needle due to high viscosity of the solution. To overcome that obstacle, we chose weight: weight ratio of the polymer and solvent. For instance, 13.5 g of DMF was added onto 1.5 g of PAN which become 10 wt. %. Applied voltage and the distance between collector to

needle greatly affects the fiber morphology. If the applied voltage is higher, it could produce coagulation and beads during fiber formation as illustrated on Figure 3.8 and Figure 3.9, respectively.

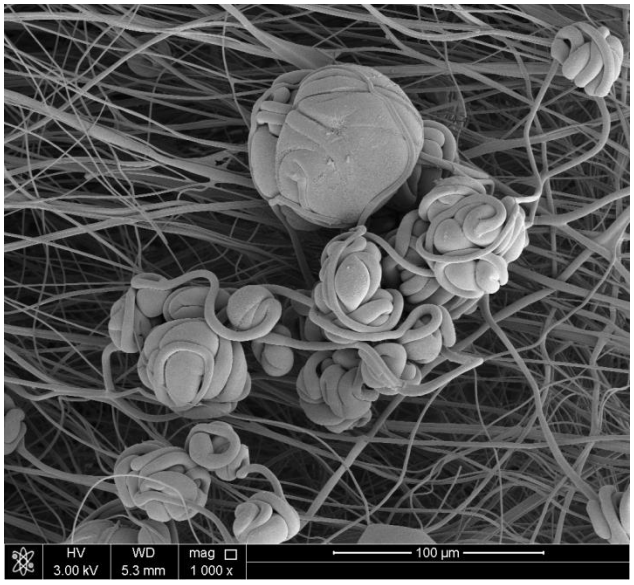

Figure 3.8: Formation of coagulation of electrospun fibers

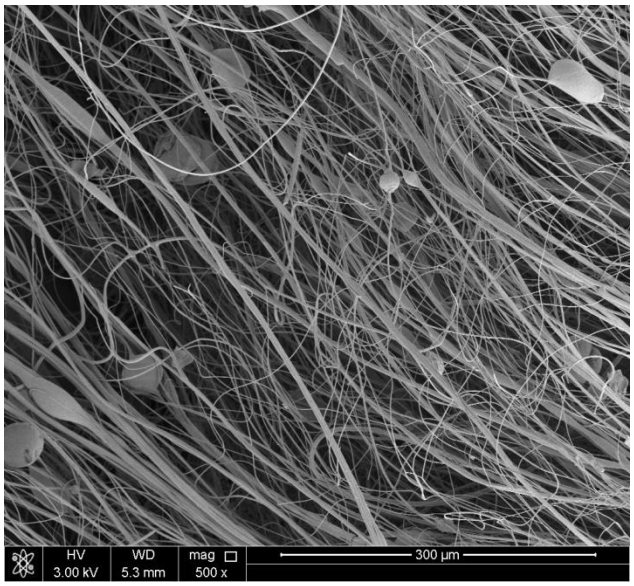

Figure 3.9: Beads formation of electrospun fibers

After successfully preparing of pure PAN fibers, we added sulfur on the PAN at 1 wt. % which was supposed to be the source of sulfur dopant after carbonization. Unfortunately, the formation of continuous fibers was failed due to the blockage on needle by sulfur particles. Figure 3.10 shows the formation of non-continuous fibers and coagulation due to the presence of sulfur particles.

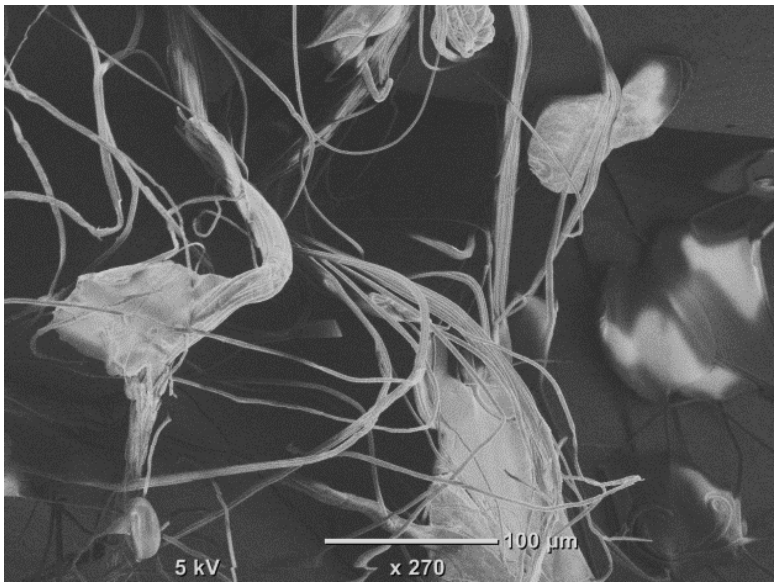

Figure 3.10: Coagulation of sulfur particles on polymer fibers

To get rid of this difficulty, we decided to use a sulfur compound (Thiophene) as a source of sulfur and urea as a source for nitrogen. We successfully synthesized the fibers although having non-uniform diameters for pure thiophene doped (Figure 3.11) which could be due to the volatilization of thiophene by electrostatic force during electrospinnig. Figure 3.12 shows Urea (source of nitrogen) and thiophene (source of sulfur) fibers with relatively good morphology and fibers were attached to each other.

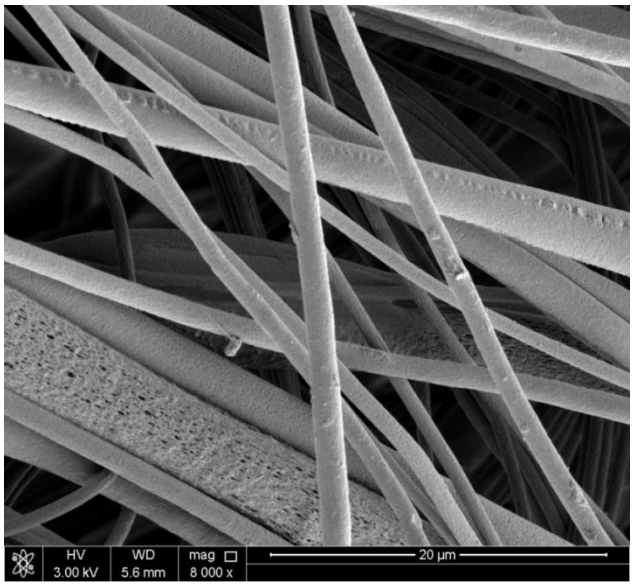

Figure 3.11: Thiophene doped PAN fibers

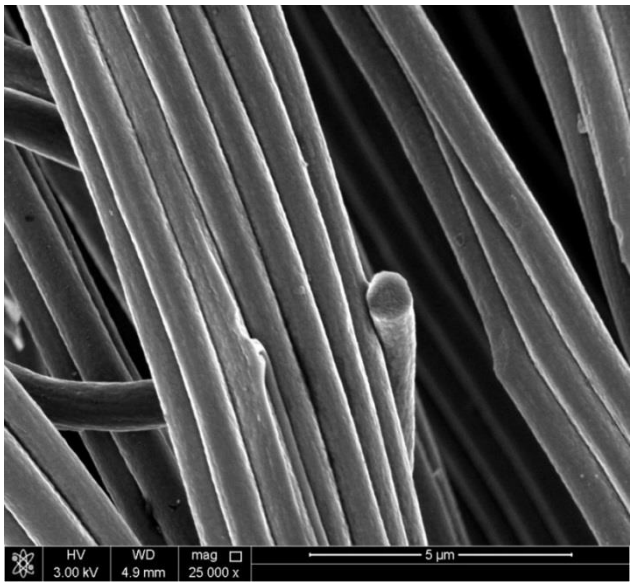

Figure 3.12: Thiophene and Urea doped PAN fibers

The formation of fibers was sucessfully done, whereas the carbonized fibers found to have no sulfur content which could be due to the formation of H_2S during carbonization at high temperature. But the carbonaceous materials ended with high nitrogen doping (12.76 %). Even though the material showed high nitrogen doping, which is a positive side of our findings, the absence of sulfur impeded achievement of our final goal. Figure 3.13, Figure 3.14, and Figure 3.15 shows deconvoluted C 1s, O 1s, and N 1s XPS peaks of Thiophene and urea doped CNF. Table 3.1 represents the atomic composition, binding energy for respective elements of Thiophene and urea doped CNF .

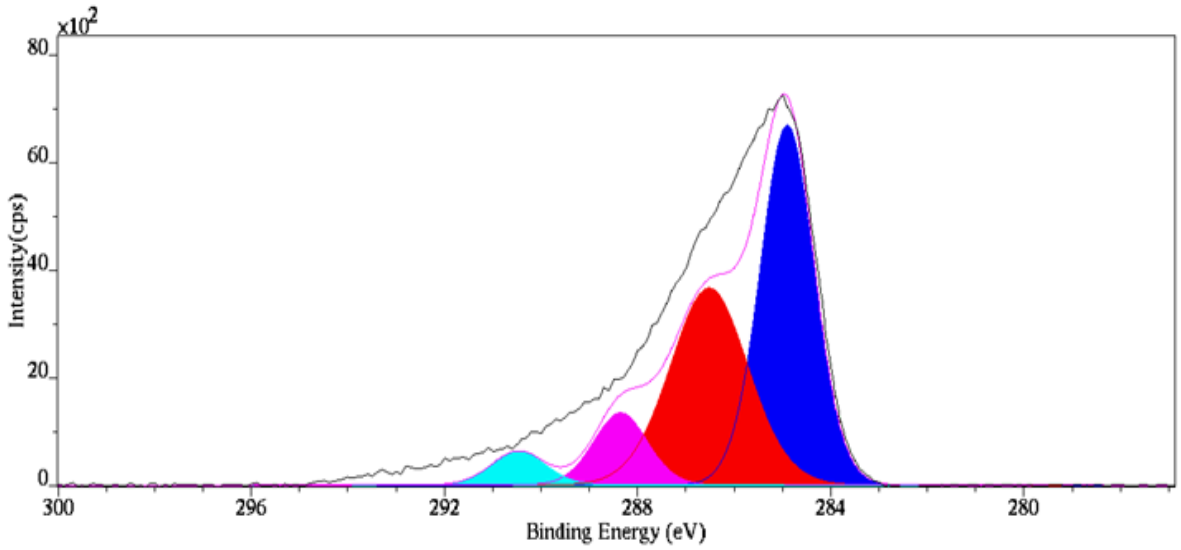

Figure 3.13: Deconvoluted C 1s XPS peak of Thiophene and urea doped CNF

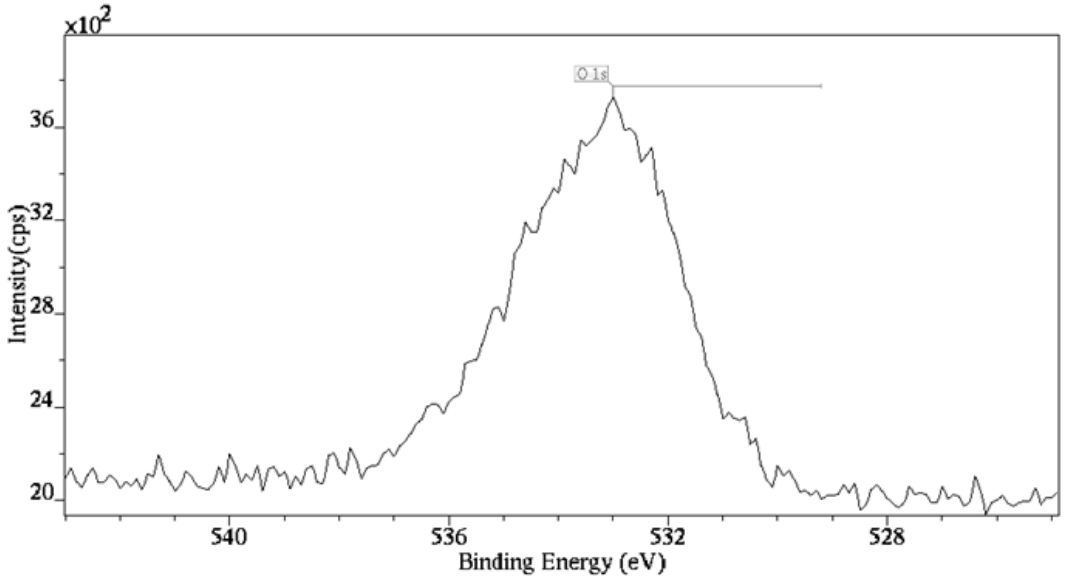

Figure 3.14: Deconvoluted O 1s XPS peak of Thiophene and urea doped CNF

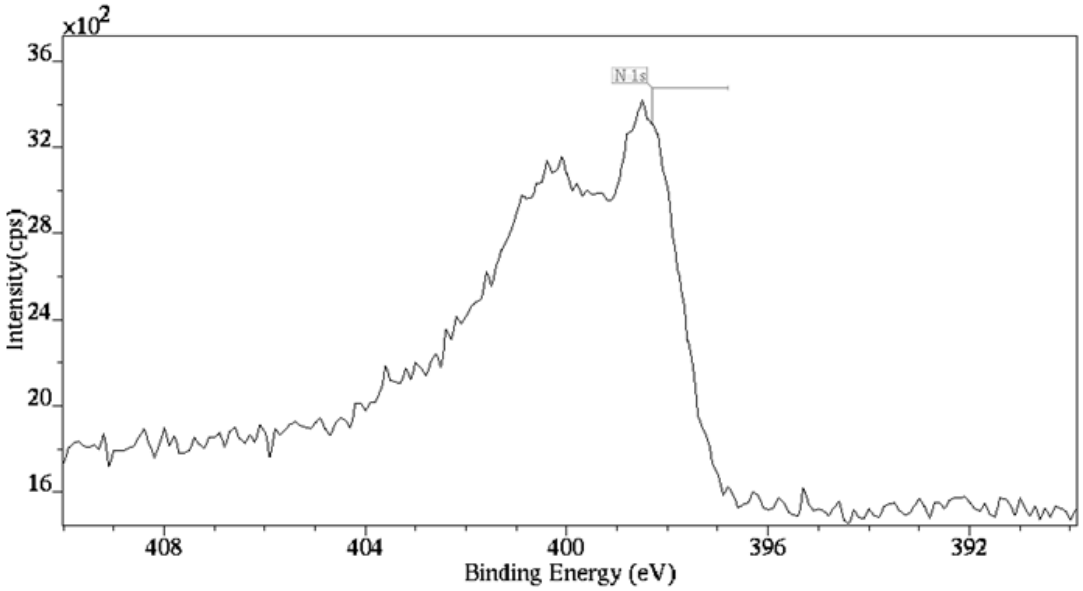

Figure 3.15: Deconvoluted N 1s XPS peak of Thiophene and urea doped CNF

Table 3.1: Elemental composition of Thiophene and urea doped CNF

Sample Id.	Peak	BE (eV)	Content (atom. %)
CNF (Thiophene and Urea doped)	C 1s	285	81.73
	N 1s	399	12.76
	O 1s	532	5.51

To achieve the desired goal, we again changed the source of sulfur and nitrogen to thiourea. Thiourea is a compound that is a source for both nitrogen and sulfur. We selected 5 different wt. % of Thiourea (1, 3, 5, 10 and 20 wt. %) on PAN at 10 wt. %. These were prepared successfully without any obstacle.

3.3 Synthesis of polymer fibers

The preparation of polymer fibers was achieved by dissolving PAN in dimethyl formamide (DMF) solvent. Different loading of Thiourea concentration as a source of nitrogen and sulfure were also prepared. Table 3.2 shows the wt. % of constituents used during the preparation of polymer solutions.

Table 3.2: Materials wt. % used during the preparation of polymer solutions

Polyacrylonitrile (PAN) (g)	**Thiourea (g)**	**Thiourea loading (%)**	**DMF (g)**
1.5	0	0	13.5
1.485	0.015	1	13.5
1.455	0.045	3	13.5
1.425	0.075	5	13.5
1.35	0.15	1	13.5
1.2	0.3	20	13.5

Table 3.3 summarizes the parameters applied during electrospinning process. After the preparation of polymer fibers, the fibers was collected from the rotating drum and dried in vacuum oven at 50 ºC for 8 hours to remove all the moisture from the fiber mat.

Table 3.3: Applied parameters during the electrospinning technique

Parameters	**Conditions**
Voltage	15 kV
Flow rate	1 ml/h
Needle diameter	0.07 mm
Rotating drum speed	200 Rpm
Tip to needle's distance	15 cm

3.4 Stabilization of polymer fibers

Prior to carbonization, the fiber mat was stabilized at 275 ºC under air. The temperature was ramped up at the rate of 2 ºC/min for 2 hours.

3.5 Carbonization of stabilized fibers

Carbonization was carried out at 800 ºC for 5 hours followed by 1000 ºC for 2 hours at 5 ºC/min heat increment under high purity (99.999) nitrogen (N_2) atmosphere (Al-Enizi et al., 2014). Initially, the sample was placed on the tube furnace on a ceramic crucible and the tube closed from both sides. Then N_2 gas flow applied on the tube for 30 min. to purge all oxygen from the chamber. Finally, the heat treatment started which lasts for 10 hours then naturally cooled down.

3.6 Metal loading by microwave technique

After proper carbonization of different samples, metal loading of the carbon fibers was carried out by using conventional microwave technique having maximum microwave power: 800 W. The parameters were set constant for all samples.

1 microgram of CNF was crushed to powder and placed on a conical flask. Then distilled water (DW) was added and dispersed by sonication method for 2 hours. Different metal sources, namely Ruthenium (III) chloride hydrate, Tin (II) chloride dehydrate and Nickel (II) acetate tetra hydrate, were also dissolved DW in according to the 1:1:1 ratio in another beaker. Then both solutions were mixed and dispersed for 1 hour. Prior to

microwave heat treatment 15 microliter of hydrazine hydrate solution was added to the mixture and sonicated for 1 min.

Microwave treatment was given for 20 sec. and the sample then for 10 sec. sonication. This process is continued for 9 times, a total time of 3 min. microwave irradiation. Then the solution was kept to cool down to room temperature. Finally, the metal loaded fibers were collected by centrifugal process at 5000 rpm for 2 hours and washed with ethanol and dried at oven overnight.

To distinguish between synthesized samples, we titled them according to the loading of Thiourea stated as follows:

Table 3.4: Designation of samples presented in this work

Thiourea loading	**Polymer fibers**	**Carbonized fibers**	**Metal loaded carbonized fibers**
0 %	PAN	Pristine/ pure CNF	M-Pristine-CNF
1 %	PAN-T-1%	CNF -T-1%	M-CNF -T-1%
3 %	PAN-T-3%	CNF -T-3%	M-CNF -T-3%
5 %	PAN-T-5%	CNF -T-5%	M-CNF -T-5%
10 %	PAN-T-10%	CNF -T-10%	M-CNF -T-10%
20 %	PAN-T-20%	CNF -T-20%	M-CNF -T-20%

3.7 Preparation of electrode for electrochemical test

Accurate result of the electrochemical test depends on the proper preparation of the working electrode. Glassy carbon is one of the commonly used electrodes to measure the electrochemical properties of supercapacitor materials.

A small amount (10 micro gram) of prepared carbon materials was weighed on small vessel, then 0.8 ml of iso-propanol and 0.2 ml of Nafion solution were added to the materials. The mixture was then dispersed by using bath sonication for at least 1 hour. From the prepared suspension, 20 micro-liters were taken by micropipette and drop casted on the glass carbon. The castings were dried at room temperature for 2 hours.

When the working electrode was ready, it rinsed with small amount of electrolyte solution (Na_2SO_4) to enhance the wettability. Then it was immersed in Na_2SO_4 solution inside the Dr. Bob cell. As the counter and reference electrode, a platinum wire and a calomel electrode were used respectively. After immersion of all electrodes, the solution was bubbled with high purity nitrogen gas for 15 min to confirm the removal of oxygen from the solution and the cell was covered with Para film to avoid air circulation. Figure 3.17 demonstrates the employed electrochemical setup during the whole experiment.

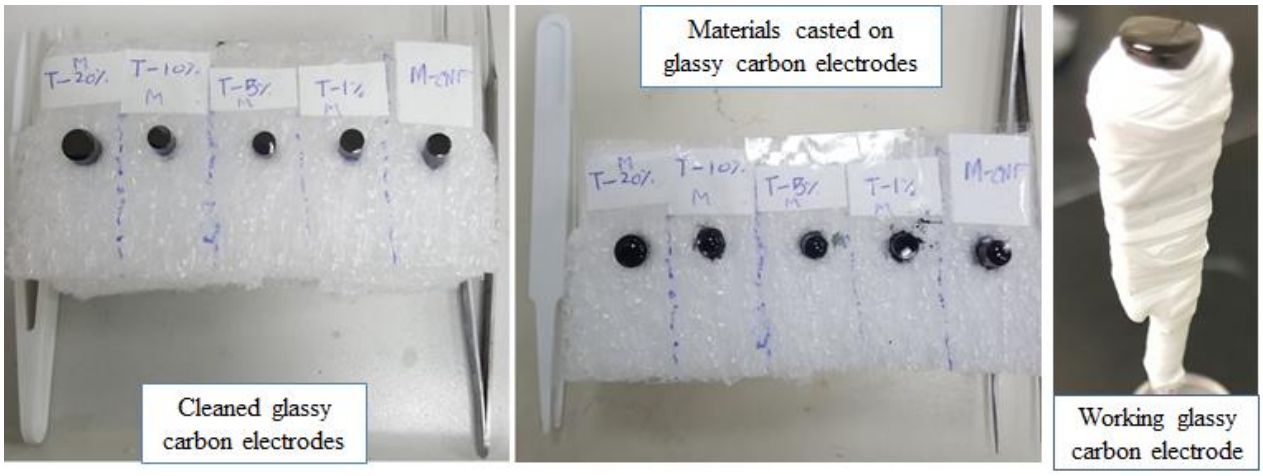

Figure 3.16: Glassy carbon electrodes before and after deposition of CNFs composite material

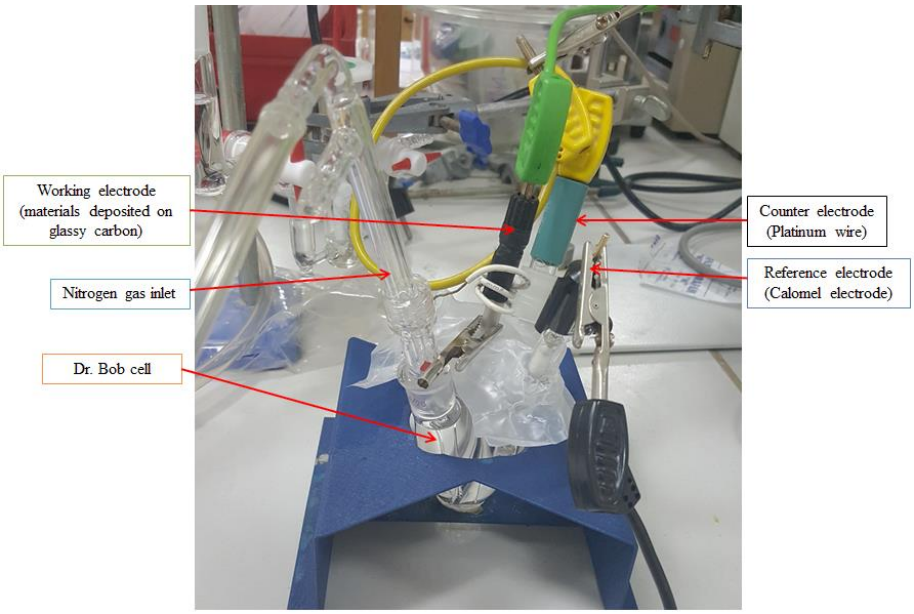

Figure 3.17: Electrochemical cell setup

Chapter 4

Results and Discussion

4.1 Morphological analysis

4.1.1 Scanning electron microscopy (SEM) results

Figure 4.1 to Figure 4.6 show the SEM micrographs of pristine, thiourea (1, 3, 5, 10, and 20 wt. %) doped PAN polymer fibers respectively. As observed from the images, fibers are randomly oriented and sometimes joined with each other, the width of the fibers ranging from 0.6 to 1.8 micro-meter. Furthermore, the fibers are showing smooth and straight shape which was ascribed to the increased PAN solution concentration up to 10 wt. % (D. Zhang et al., 2009). The length of the electrospun fibers are on the order of few centimeters.

Figure 4.7 to Figure 4.9 shows the carbonized fibers of pristine, Thiourea 1, and 5 wt. % carbon fibers. It is noticeable that the thickness of the fibers are ordinarily reduced after the carbonization process due to the removal of non-carbon volatile materials during high temperature treatment. The average diameter of the carbon fibers ranged from 0.3 to 1 micro-meter. Pristine PAN fibers showed broken morphology, whereas CNF-T-5%, and CNF-T-10% carbon fibers showed continuous morphology. Moreover, some irregular pores can be observed on the surface of CNF-T-10% fibers.

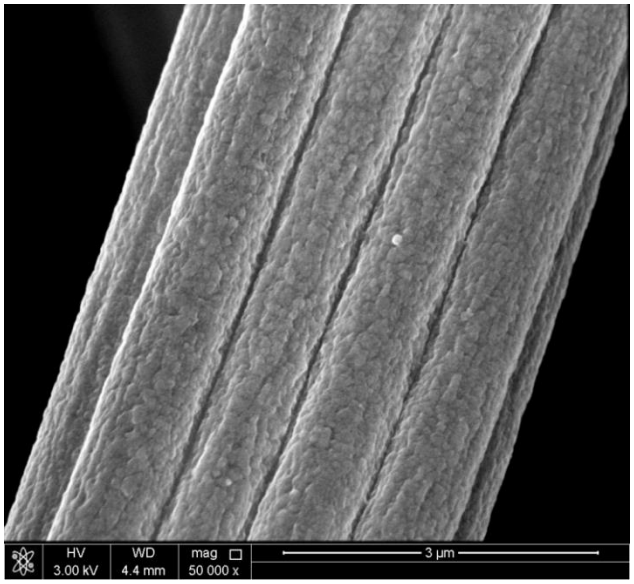

Figure 4.1: SEM micrograph of PAN electrospun fibers

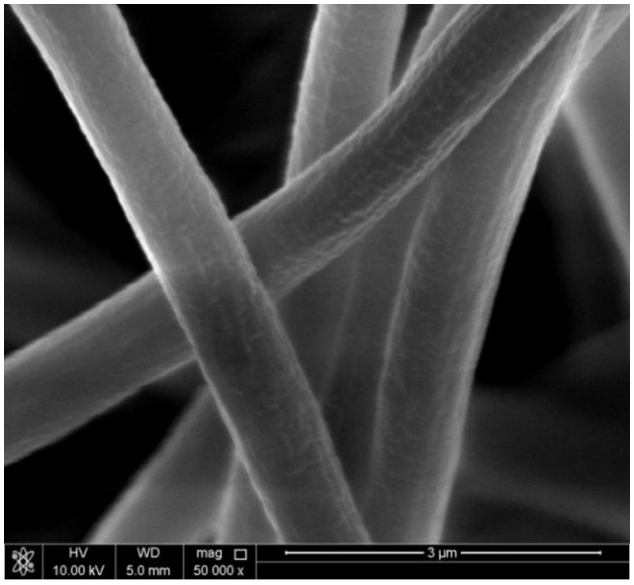

Figure 4.2: SEM micrograph of PAN-T-1% fibers

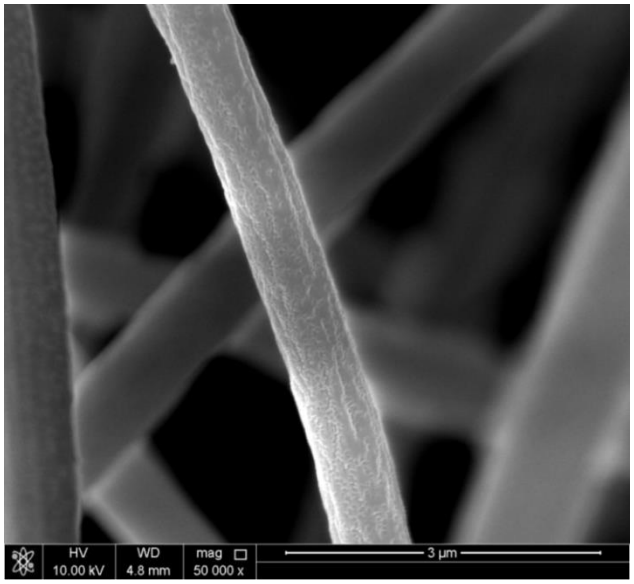

Figure 4.3: SEM micrograph of PAN-T-3% fibers

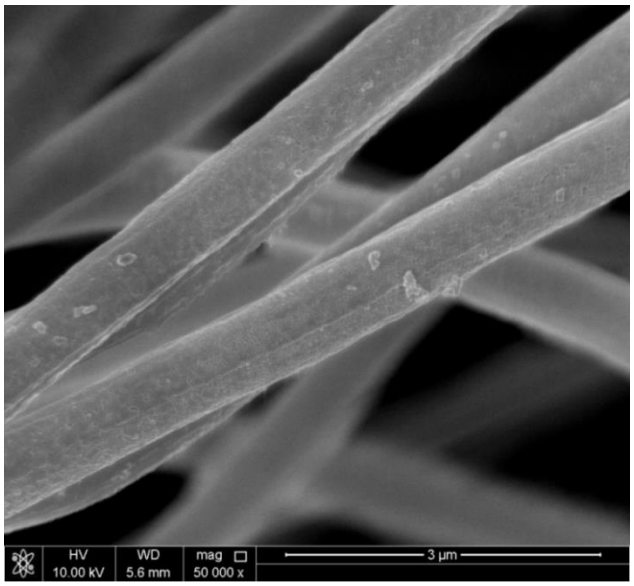

Figure 4.4: SEM micrograph of PAN-T-5% fibers

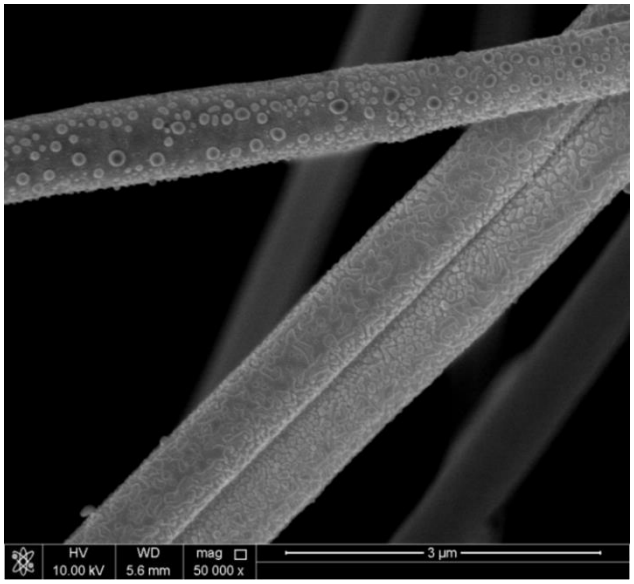

Figure 4.5: SEM micrograph of PAN-T-10% fibers

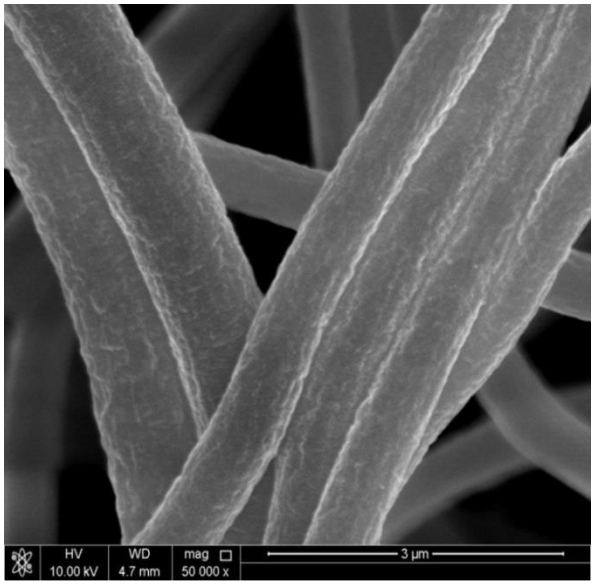

Figure 4.6: SEM micrograph of PAN-T-20% fibers

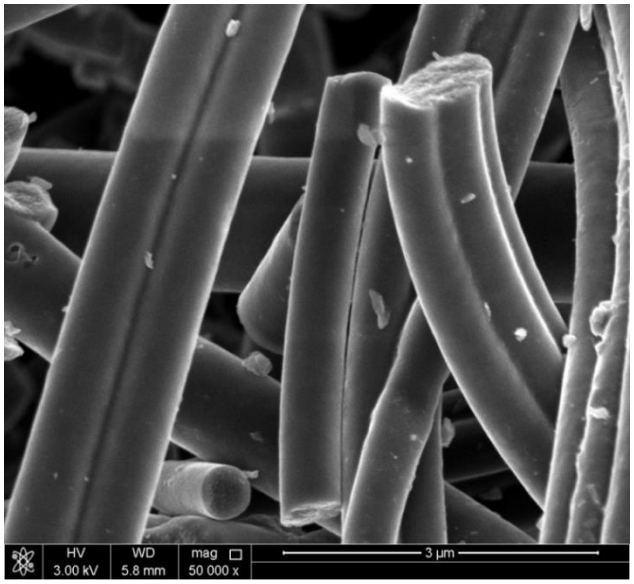

Figure 4.7: SEM micrograph of pristine CNF

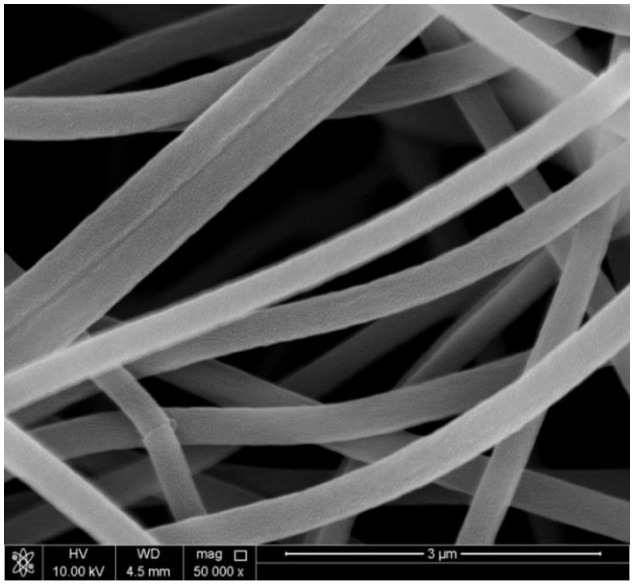

Figure 4.8: SEM micrograph of CNF-T-5% fibers

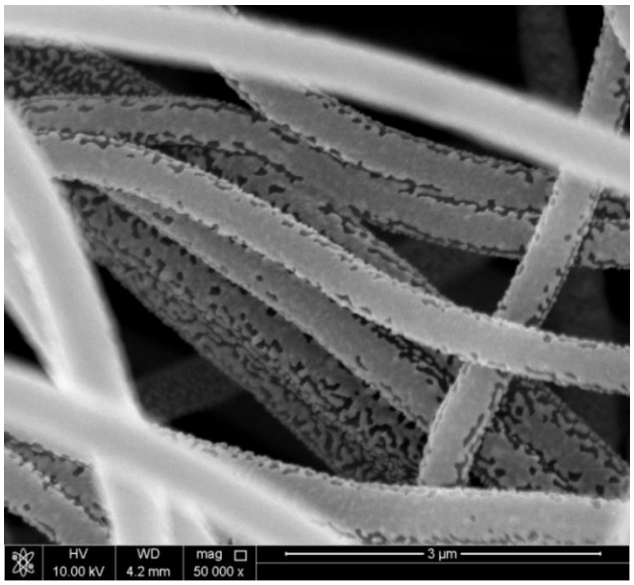

Figure 4.9: SEM micrograph of CNF-T-10% fibers

4.1.2 Transmission electron microscope (TEM) results

The high resolution TEM micrographs from Figure 4.10- Figure 4.13 represents the microwave assisted metal loaded doped carbon fibers. As observed from the images, the metal particles are deposited on the surface of the carbon fibers. The distributions are random and not covering all the surface of the CNFs. As observed from the images, the size of the particles lies between 100 and 200 nm.

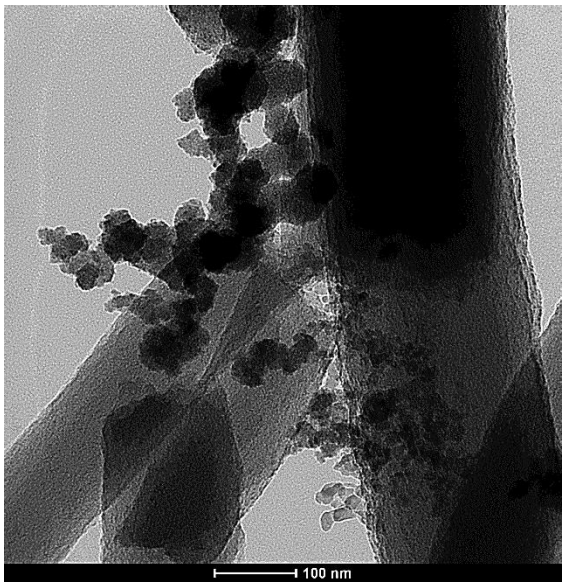

Figure 4.10: TEM micrograph of M-CNF sample

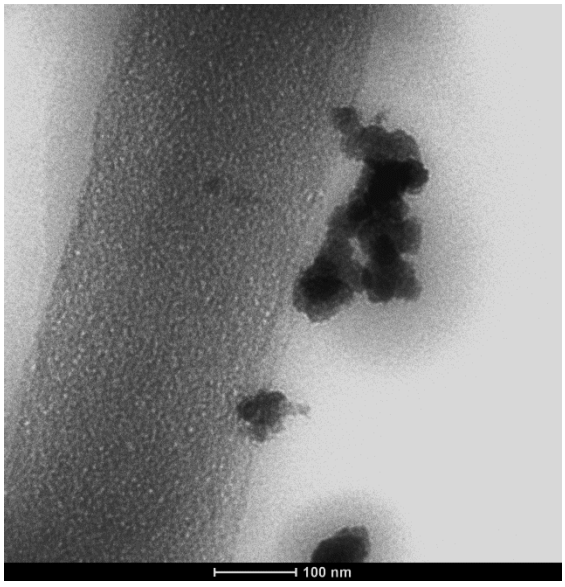

Figure 4.11 TEM micrograph of M-CNF-T-1% sample

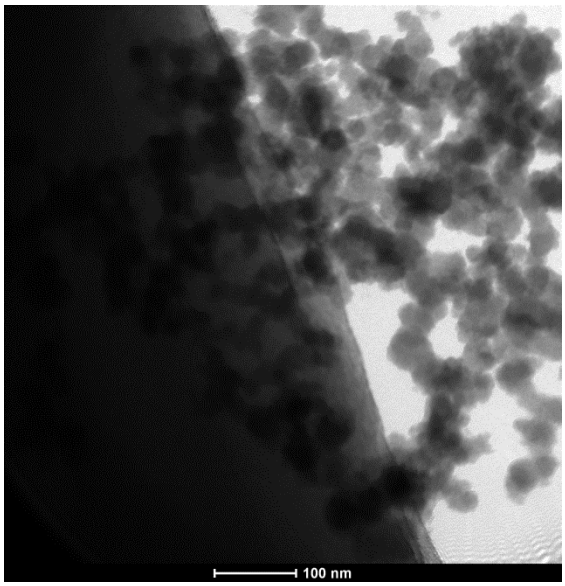

Figure 4.12 TEM micrograph of M-CNF-T-10% sample

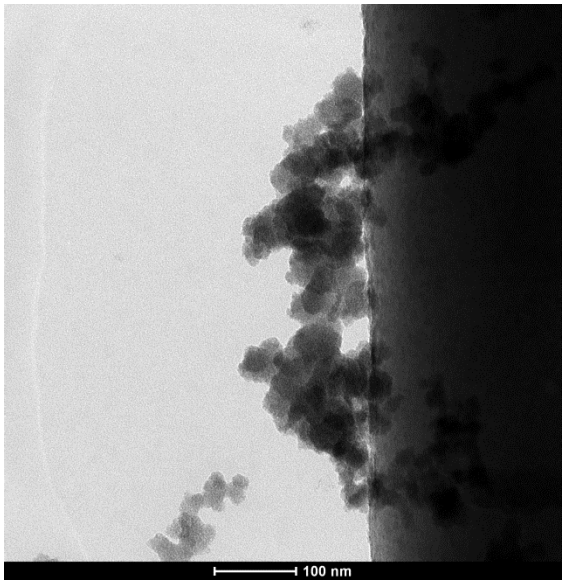

Figure 4.13 TEM micrograph of M- CNF-T- 20% sample

4.2 Structural analysis

4.2.1 FTIR analysis

FTIR of various samples were performed to confirm the changes happened after the addition of Thiourea. The FTIR spectra of PAN and Thiourea powder samples are shown in Figure 4.14. The various absorption band in FTIR spectra and the corresponding assignments are given below.

The frequencies at 2930, 2242, 1628, 1455, 1361 cm^{-1} for PAN due to the stretching of C≡N, bending of CH_2, stretching of CN, stretching of CH_2 and bending of C-H vibrations respectively (Jing et al., 2007). The frequencies at 1620, 1417, 1089, 731 cm^{-1} for Thiourea due to the bending of NH_2, asymmetric stretching of C=S, stretching of C=S and symmetric stretching of C=S respectively (Madhurambal, Mariappan, & Mojumdar, 2010). Both of the sample shows the characteristic vibration frequencies of respective substances.

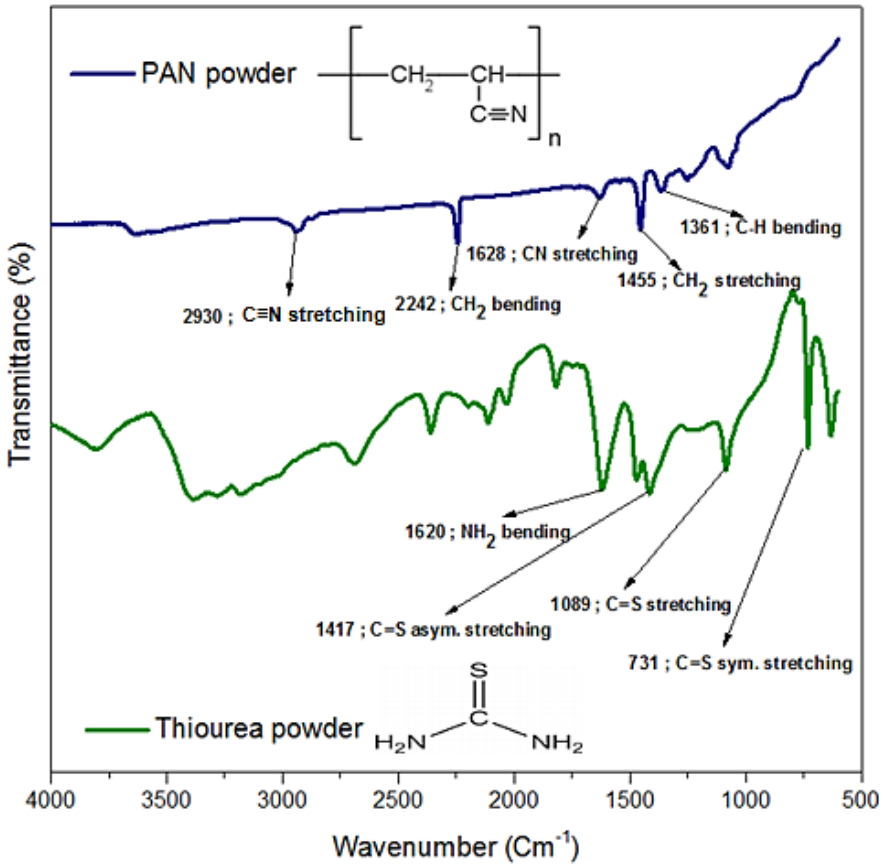

Figure 4.14: FTIR assignments for PAN and Thiourea powder

The various absorption band in FTIR spectra and the corresponding assignments at Figure 4.15 are belongs to PAN and PAN+ Thiourea electrospun fibers respectively. the additional peaks at 1089 and 731 cm^{-1} in PAN+ Thiourea sample corresponds to C=S stretching and C=S symmetric stretching respectively. This confirms the presence of Thiourea on PAN electrospun fibers.

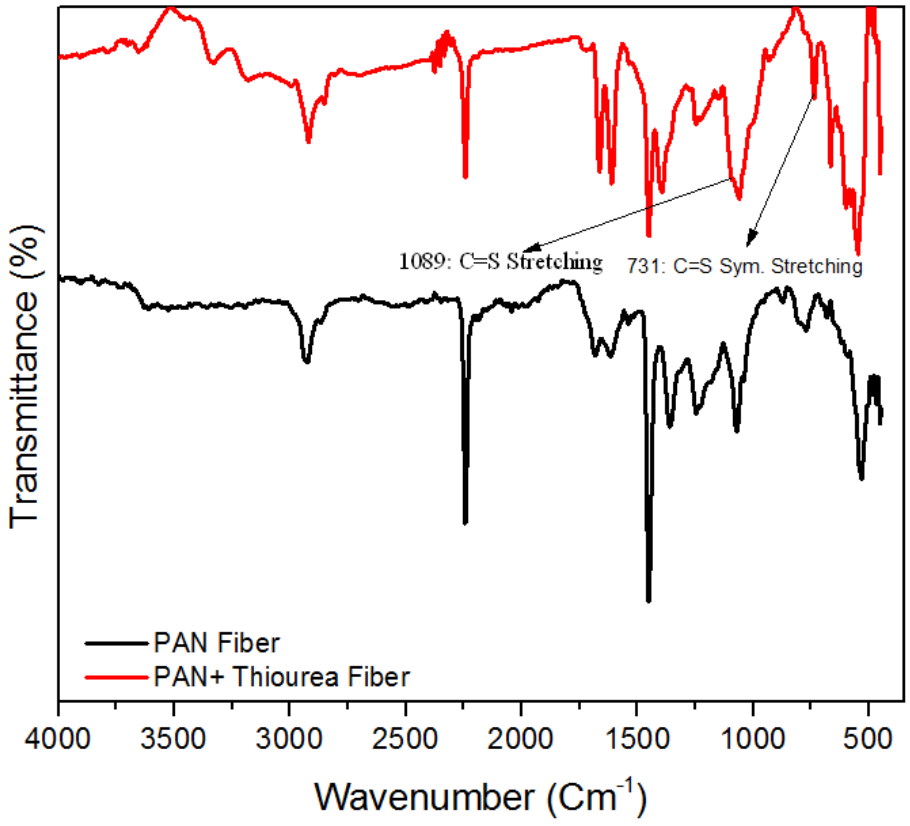

Figure 4.15: FTIR assignments for PAN and PAN+ Thiourea electrospun fiber

4.3 Spectroscopy:

4.3.1 X-ray diffraction spectroscopy results:

XRD analysis was performed in order to confirm the metal loading on CNFs. A significant change has been observed on 500 ^{o}C annealed metal loaded CNFs. Figure 4.16 represent the powder pattern of pristine CNFs. The XRD pattern of the pristine CNFs exhibits a broad diffraction peak at around 25^{o} corresponding to the (002) plane of the graphitic carbon (Al-Enizi et al., 2014). The diffraction peak at 25^{o} in M-CNFs sample confirms the presence of carbon supports along with Ru, Sn, and Ni nanocomposites. As demonstrated from Figure 4.18 and Figure 4.19, the diffraction peaks in Figure 4.17 at 2θ = 22, 38, 44.6, 65 and 78^{o} corresponding to (110), (200), (101), (202) and (321) planes respectively (Fu, Li, & Xu, 2014; Zhu et al., 2015)

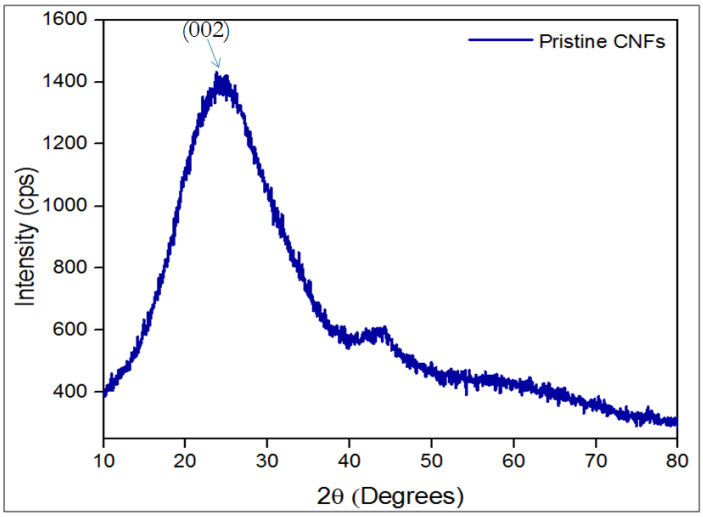

Figure 4.16: XRD pattern of carbonized CNF

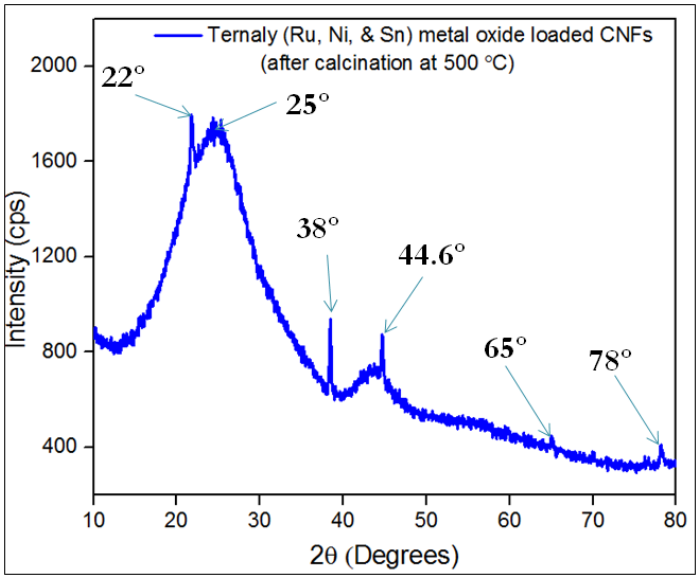

Figure 4.17: XRD pattern of metal loaded annealed CNFs

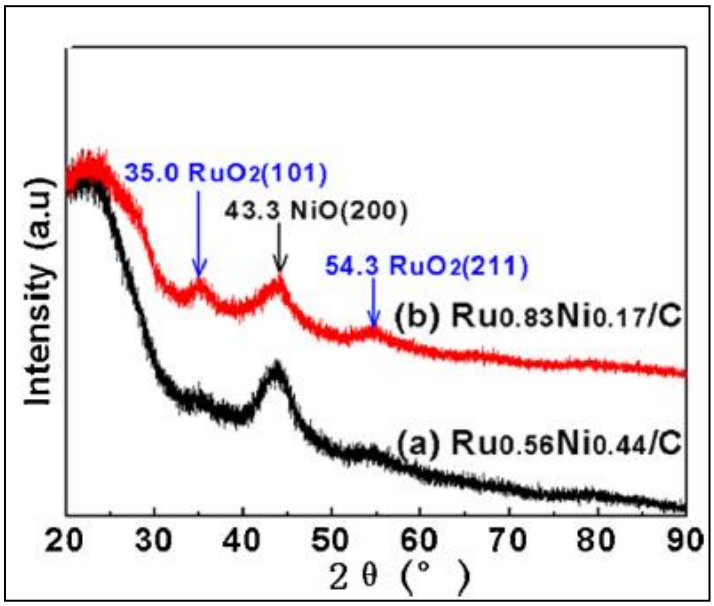

Figure 4.18: XRD patterns of Ru and Ni oxides (Fu, Li, & Xu, 2014)

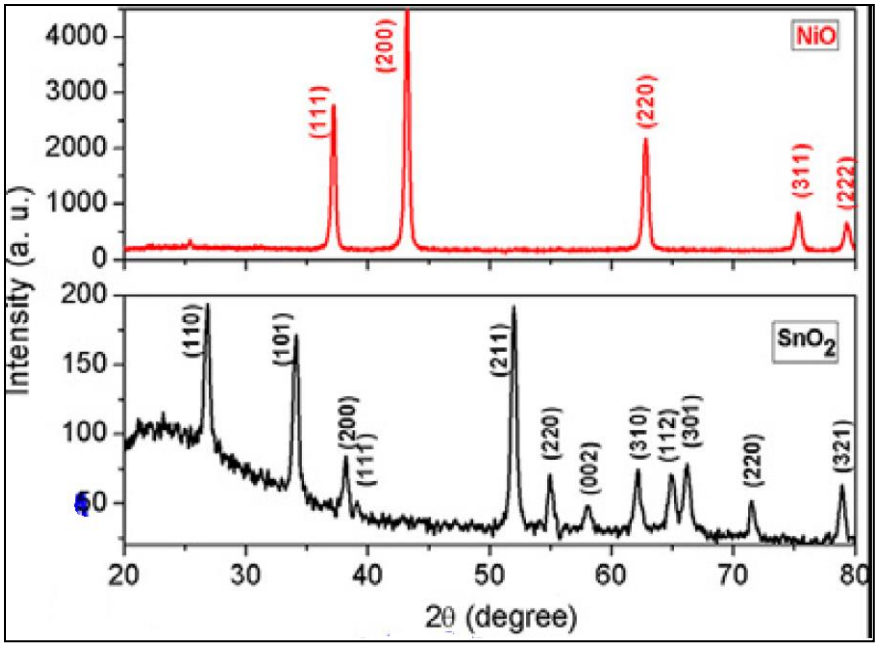

Figure 4.19: XRD patterns of nickel and tin oxide (Zhu et al., 2015)

4.3.2 Energy dispersive X-ray (EDX) analysis:

EDX analysis data at Figure 4.20 confirms the presence of carbon and traces of nitrogen, sulfur, ruthenium, nickel and tin on the metal loaded Thiourea doped CNFs sample.

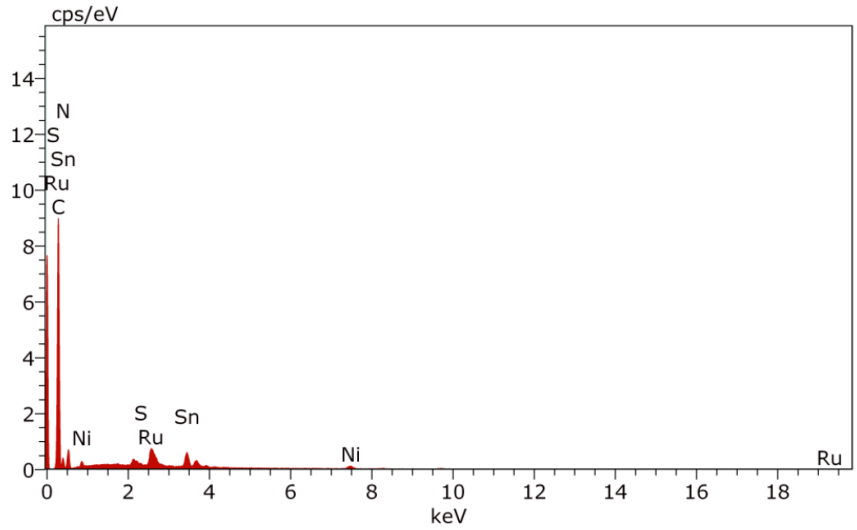

Figure 4.20: EDX elemental analysis graph

4.3.2 X-ray Photoelectron Spectroscopy (XPS) analysis

Beside morphological and structural properties, the nature and arrangement of the atoms existing in the CNFs are exceptionally essential for the supercapacitor applications. The carbon materials containing functional groups such as nitrogen, oxygen and sulfur assumed an imperative part in energy applications. Hence, the atomic arrangement of pristine CNF, doped CNFs and metal loaded CNF were investigated by XPS analysis.

In the XPS analysis all six samples (Pristine CNF, CNF-T-1%, CNF-T-3%, CNF-T-5%, CNF-T-10% and M-CNF-T-10%) confirmed the presence of carbon (C 1s peak from 281 to 285 eV), oxygen (O 1s peak at around 532 eV) and nitrogen (N 1s peak at around 401 eV). In addition, the presence of sulfur (S 2p peak from 162 to 167 eV) on the samples CNF-T-5%, CNF-T-10% and M-CNF-T-10% was demonstrated. The atomic weight

percentage of the elements presented in the samples was also determined by XPS. The values are presented in Table 4.1.

As the amount of Thiourea increases, the amount of oxygen increases but nitrogen decreases until the sample CNF-T-5%. A sudden increase in the amount of nitrogen on CNF-T-10% sample was observed. It is affirmed from the investigation that, the presence of nickel (Ni 2p at 853 eV), ruthenium (Ru 3p at 484 eV) and tin (Sn 3p at 712 eV) confirms the successful metal loading treatment.

Peak fitting was performed for C 1s and N 1s peaks of all specimens in order to investigate the atomic nature of N and O. The deconvolution of N 1s peak illustrates the existence of graphitic N (binding energy (B. E.) = 401 eV) for four samples (Pristine CNF, CNF-T-1%, CNF-T-3%, CNF-T-5%) and pyridinic (B. E. = 397 eV) for CNF-T-10% and M-CNF-T-10% samples (Wei et al., 2016). XPS analysis confirmed the presence of sulfur and pyridinic nitrogen when Thiourea doping level reached to 10 wt. %.

Table 4.1: Outline of XPS Peak analysis and quantification of N and S doped CNF materials:

Sample Id.	Peak	BE (eV)	Content (atom%)
Pure CNF	C 1s	285	95.30
	N 1s	401	2.33
	O 1s	532	2.37
	S 2p	170	0
CNF-T-1%	C 1s	285	83.30
	N 1s	402	1.20
	O 1s	532	11.50
	S 2p	165	0
CNF-T-3%	C 1s	285	95.99
	N 1s	401	2.00
	O 1s	532	2.01
	S 2p	169	0
CNF-T-5%	C 1s	281	82.83
	N 1s	400	0.99
	O 1s	529	16.16
	S 2p	164	0.01
CNF-T-10%	C 1s	284	72.07
	N 1s	397	18.13
	O 1s	530	9.72
	S 2p	162	0.08
M-CNF-T-10%	C 1s	283	58.08
	N 1s	397	3.94
	O 1s	529	21.96
	S 2p	167	0.18
	Ni 2p	853	2.81
	Ru 3p	484	6.45
	Sn 3p	712	6.59

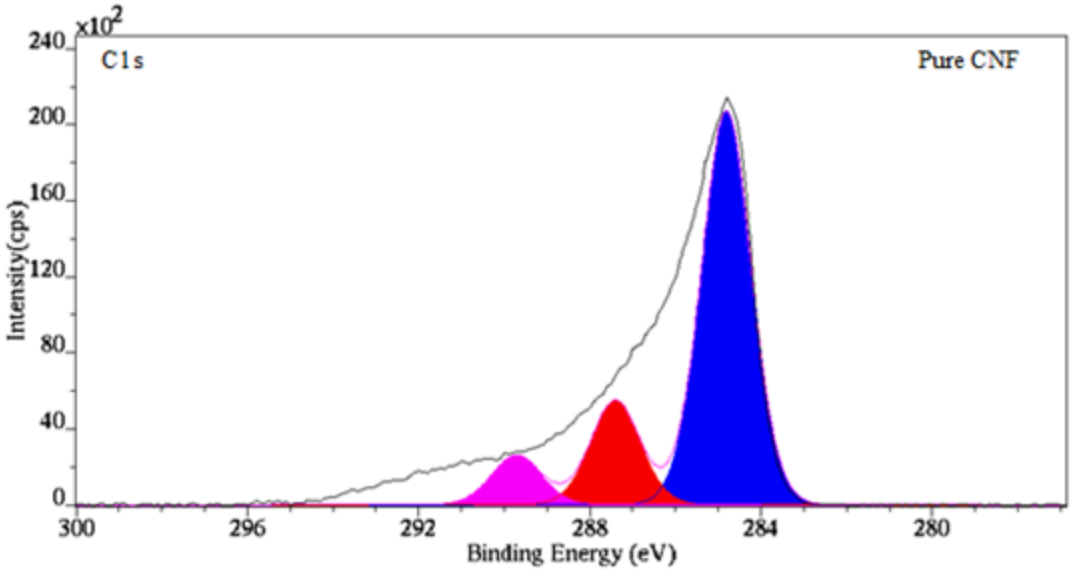

Figure 4.21: Deconvoluted C 1s XPS peaks of Pristine CNF

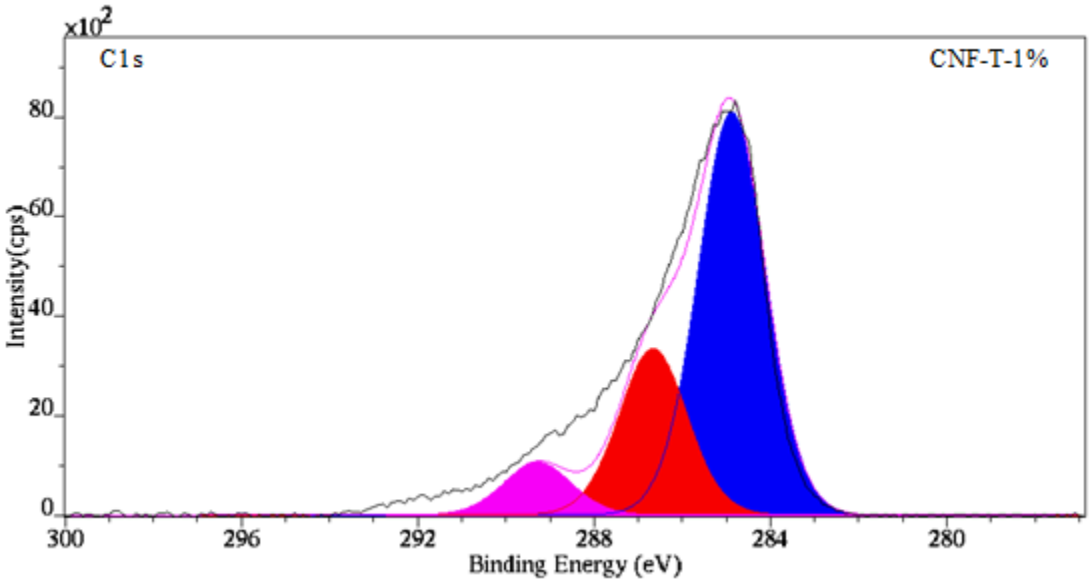

Figure 4.22: Deconvoluted C 1s XPS peaks of CNF-T-1%

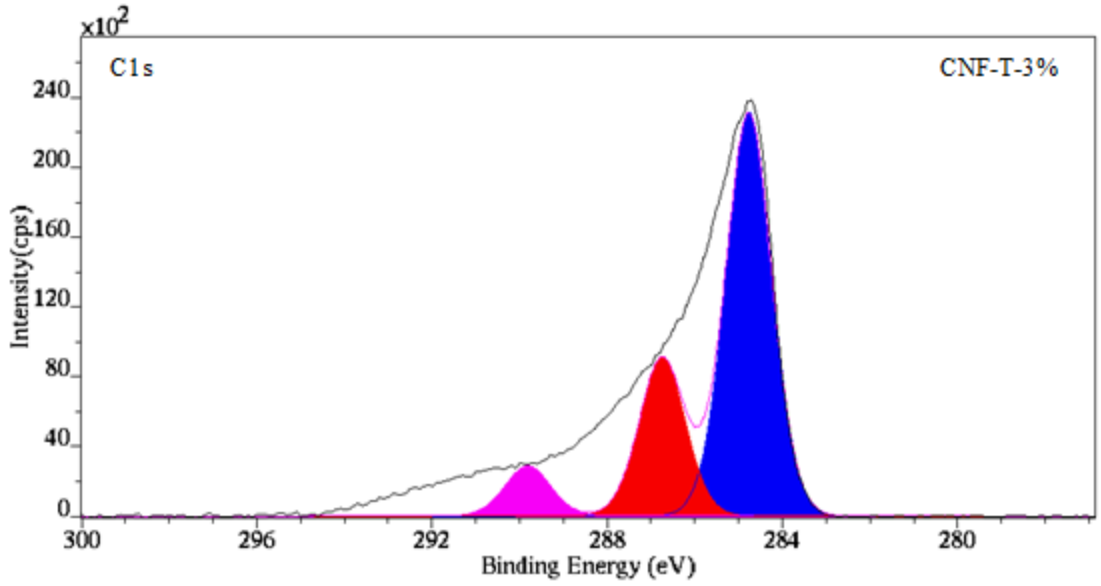

Figure 4.23: Deconvoluted C 1s XPS peaks of CNF-T-3%

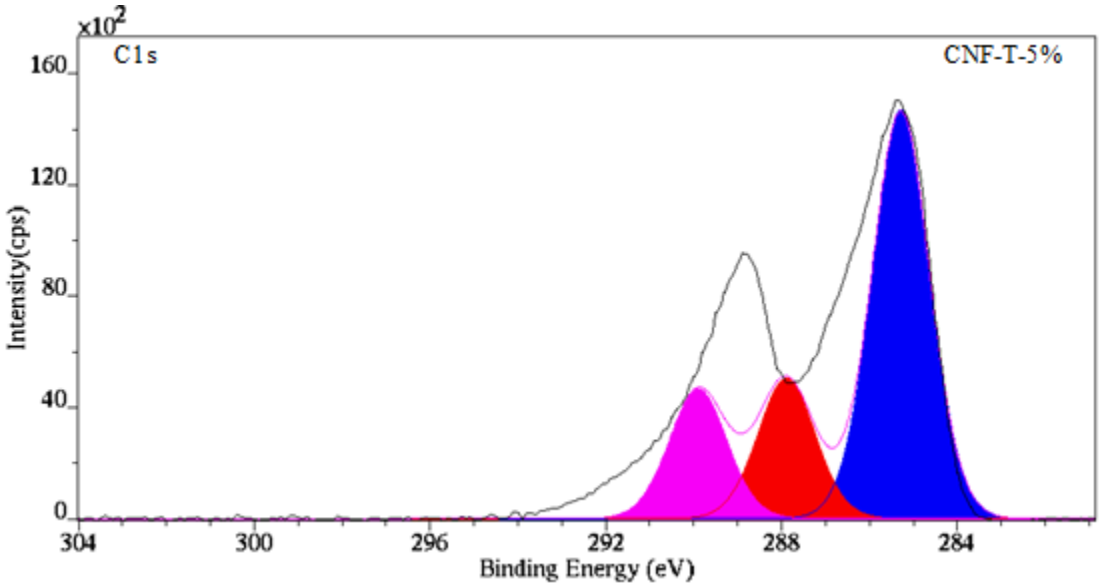

Figure 4.24: Deconvoluted C 1s XPS peaks of CNF-T-5%

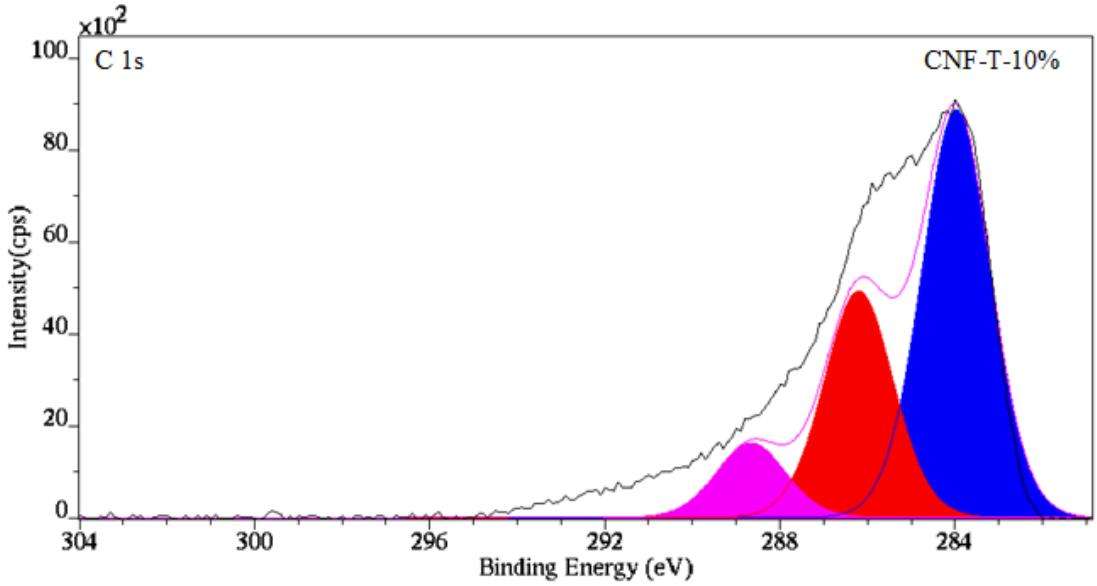

Figure 4.25: Deconvoluted C 1s XPS peaks of CNF-T-10%

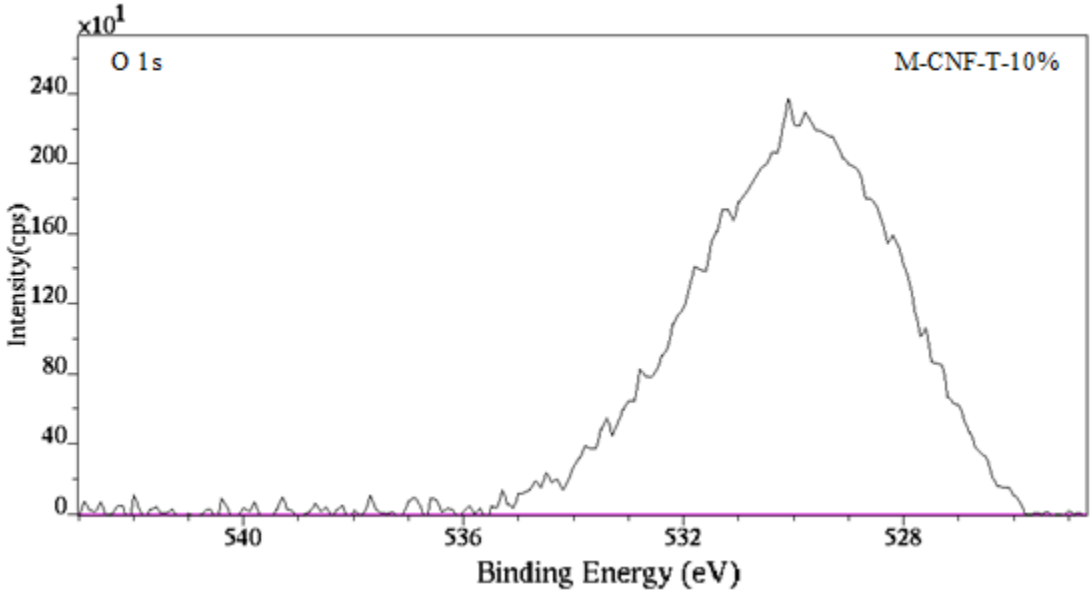

Figure 4.26: Deconvoluted O 1s XPS peak of M-CNF-T-10%

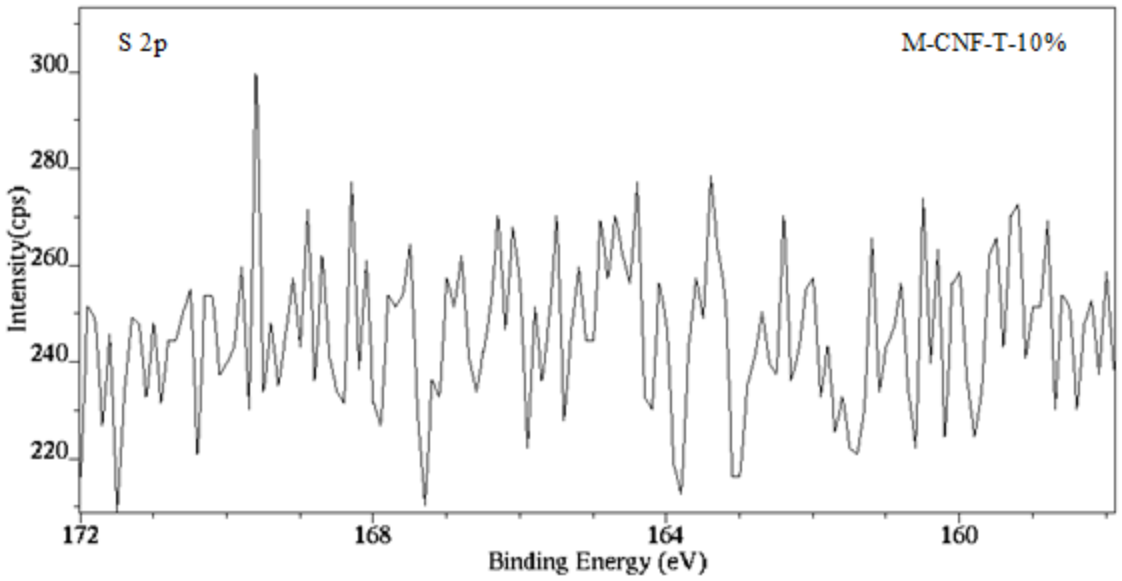

Figure 4.27: Deconvoluted S 2p XPS peak of M-CNF-T-10%

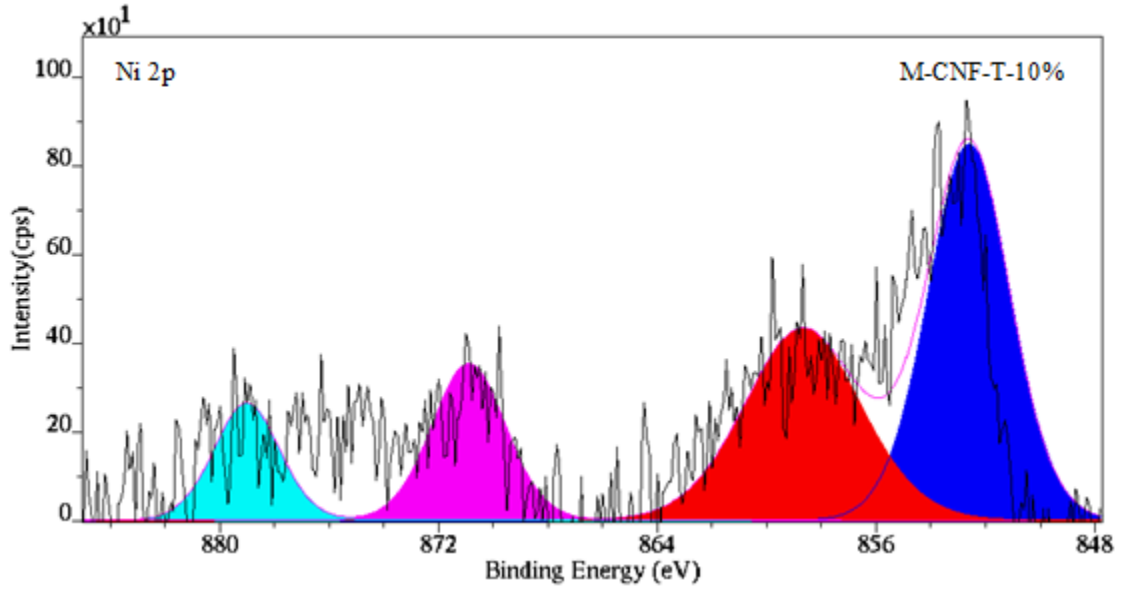

Figure 4.28: Deconvoluted Ni 2p XPS peak of M-CNF-T-10%

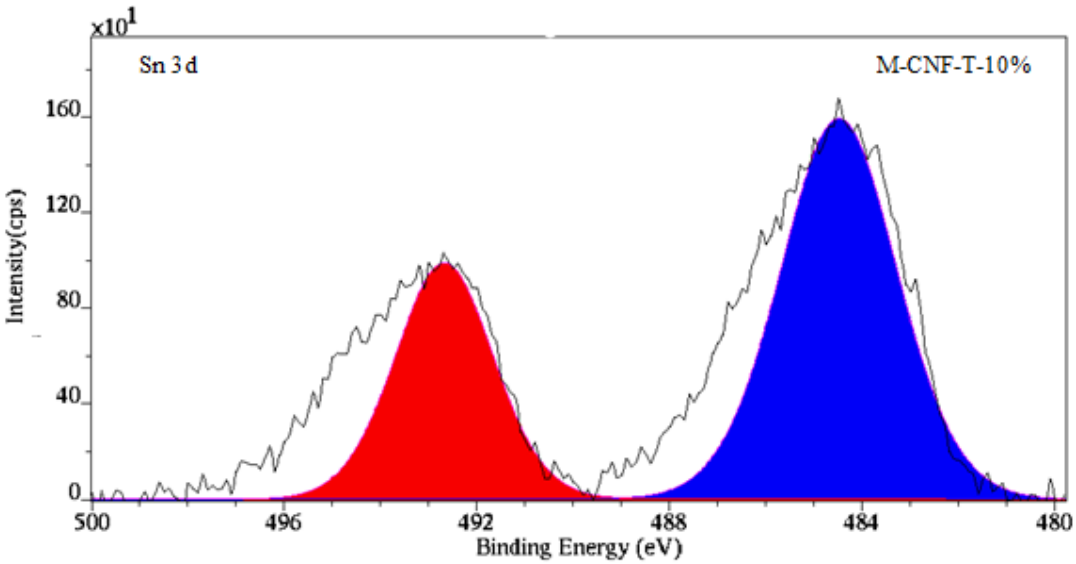

Figure 4.29: Deconvoluted Sn 3d XPS peak of M-CNF-T-10%

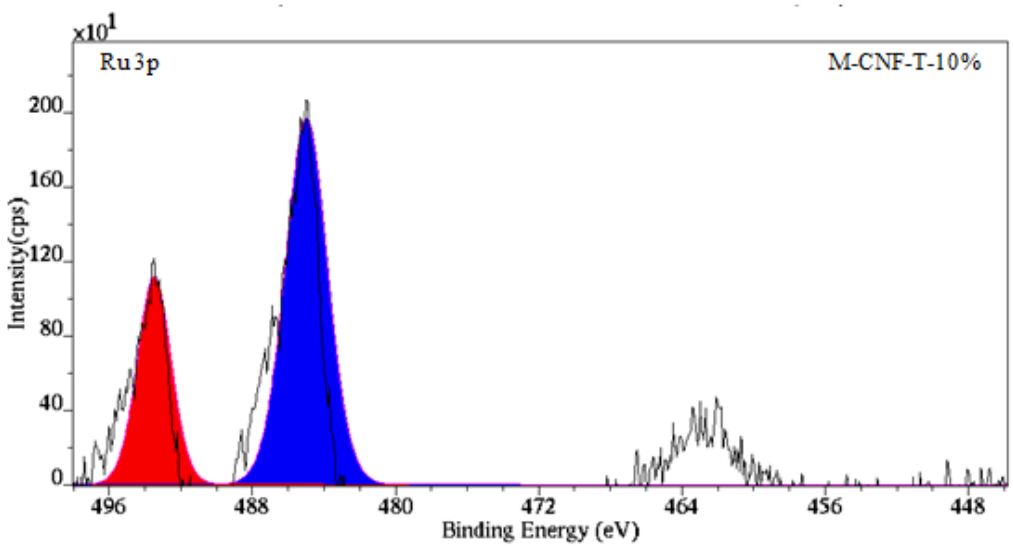

Figure 4.30: Deconvoluted Ru 3p XPS peak of M-CNF-T-10%

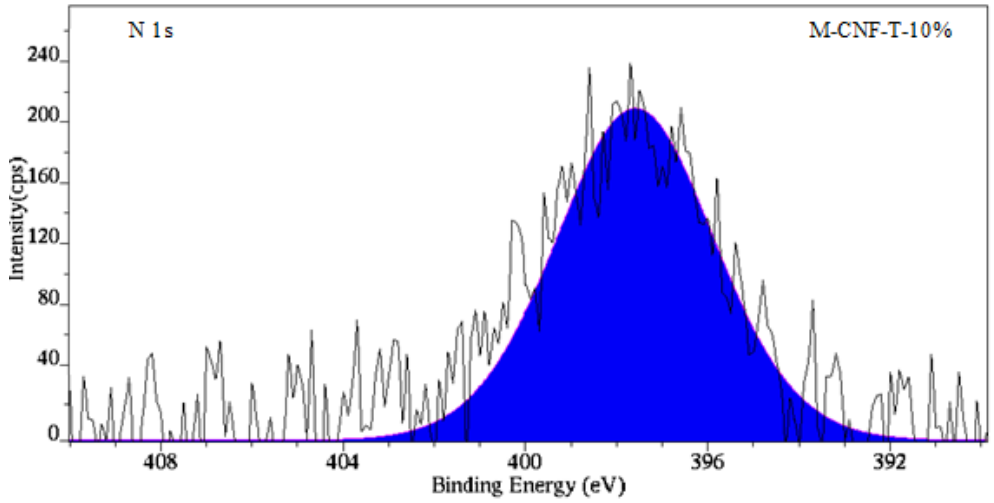

Figure 4.31: Deconvoluted N 1s XPS peak of M-CNF-T-10%

4.4 Electrochemical study

Electrochemical test is one of the important tools to measure the performance of supercapacitor electrode materials. Among electrochemical tests, cyclic voltammetry (CV) is a technique that utilizes a potential ramp or a shift and monitor the resulting current using high scan rates. In CV, an oxidation and/or a reduction currents appear at particular voltages that is dependent on the properties of the electrode and the measuring analyte.

The specific capacitance of an electrode material can be calculated by using Equation 1 (W. Chen, Fan, Gu, Bao, & Wang, 2010). Shows the description of each terminology.

$$\boldsymbol{C} = \int_{E1}^{E_2} \frac{\boldsymbol{i(E)dE}}{\boldsymbol{2(E_2 - E_1)mv}} \qquad 1$$

Equation 1: Calculation of specific capacitance

Where, C is denoted for the specific capacitance for individual sample

E_1 and E_2 are the potential difference in CV

i(E) is the applied current

$\int_{E_1}^{E_2} i(E)dE$ is the integration of positive and negative sweep of volumetric charge obtained from cyclic Voltamogram

E_2-E_1 is the width of potential window

m is the mass for individual sample used as electrode material during the measurement

Three-electrode cells setup was used to determine the specific capacitance of the electrode material. Figure 4.32- Figure 4.34 show the typical CV curves of 1, 5 and 10 wt. % Thiourea-doped metal-loaded CNF (calcined at 500 ºC) electrode material at different scan rates within a potential window of -0.6 to 1 V. All materials showed rectangle-shaped profile with redox peaks which is the characteristic of an ideal double layer capacitor (Z. Zhou & Wu, 2013).

As the scan rate increases, the cyclic voltammograms maintained its rectangular shape without an obvious distortion, even at a scan rate of 100 mV $s^{-1}$for the metal loaded 1 wt. % Thiourea doped CNF and of 500 mV s^{-1} for the metal loaded 5 and 10 wt.% Thiourea doped CNF electrode materials.

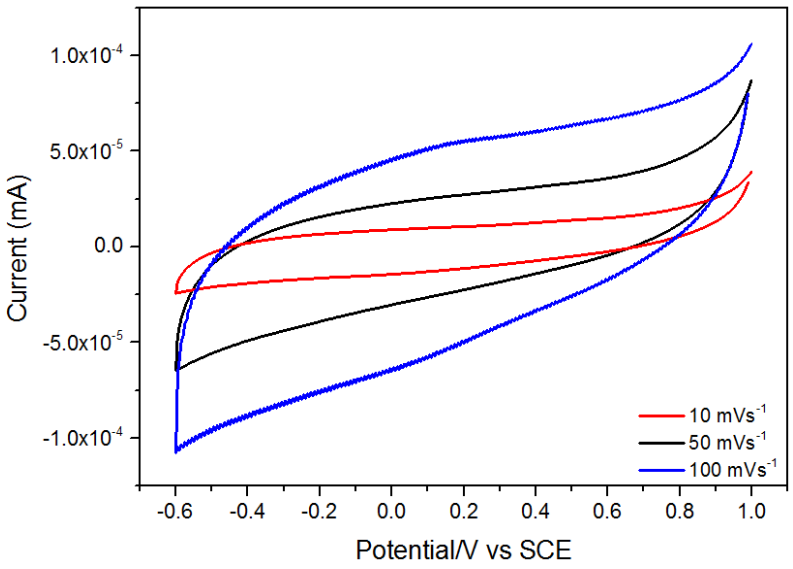

Figure 4.32: CVs of 1 wt. % thiourea doped metal loaded CNF at different scan rate

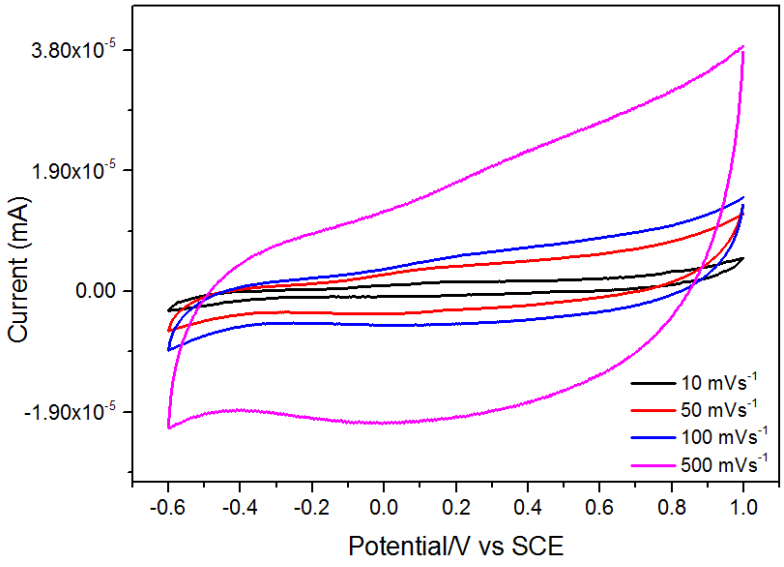

Figure 4.33: CVs of 5 wt. % Thiourea doped metal loaded CNF at different scan rate

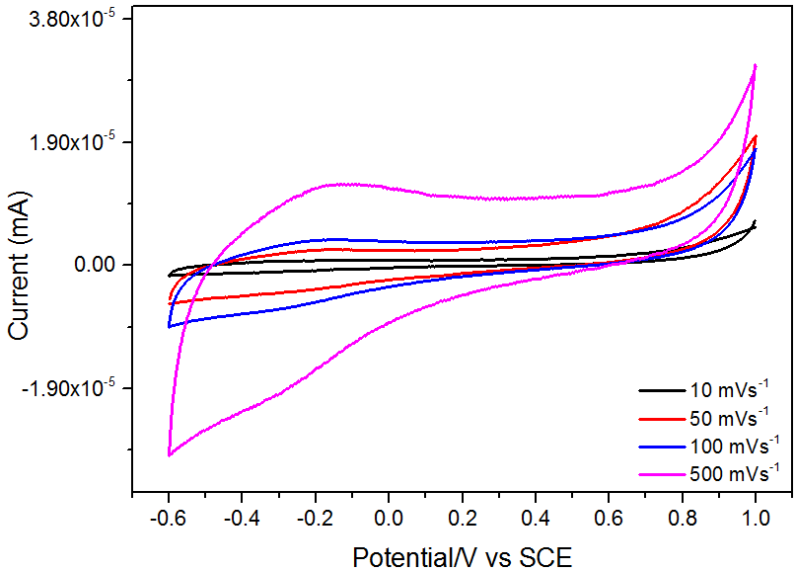

Figure 4.34: CVs of 10 wt. % Thiourea doped metal loaded CNF at different scan rate

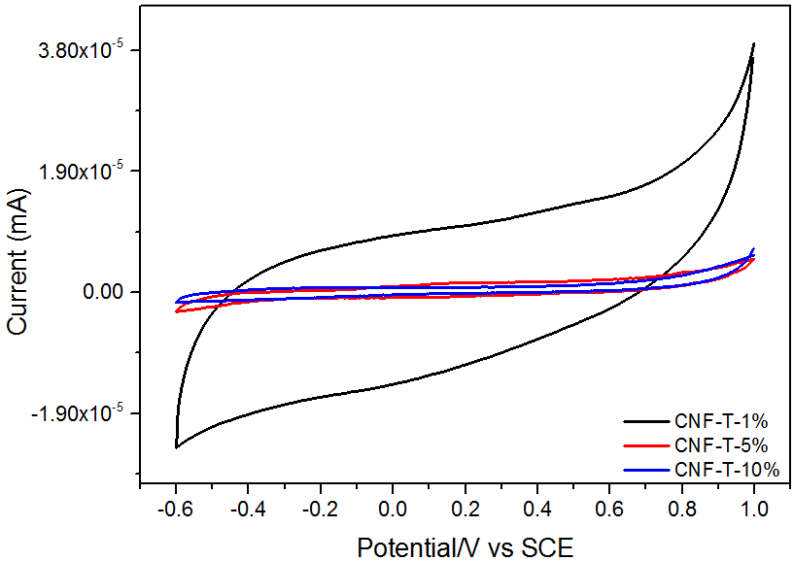

Figure 4.35: Comparison between CVs of different wt. % Thiourea doped metal loaded CNF at scan rate of 10 mVs^{-1}

Figure 4.35 shows a comparison between typical CVs of 1, 5 and 10 wt. % electrode materials. A highest specific capacitance of 207.29 F. g^{-1} was obtained at scan rate of 10 mV s^{-1} within a 1.4 V voltage window for the 1 wt. % Thiourea doped metal loaded CNF sample. Specific capacitance of 83.8 and 105.2 F. g^{-1} were obtained for 5 and 10 wt. % metal loaded CNF respectively. The electrode loading was 7.00 x 10^{-5} g. The capacitance values decreased with increasing scan rate because of mass transfer limitation at high scan rate.

Chapter 5

Conclusion

In this work, beginning from the preparation of polymer fibers by electrospinning, carbonization, and metal loading on carbon fibers were studied and concluded with an applied test on supercapacitor materials at laboratory scale. A new demonstration of sulfur and nitrogen doped carbon fibers during electrospinning process has been established. Furthermore, ternary metal deposition by microwave heat treatment has been demonstrated.

Among other investigations, XPS analysis proved a precise method to inspect the elements of carbon based materials at atomic level. To measure the performance of supercapacitor materials at laboratory scale, cyclic voltammetry measurement is well recognized.

From the above study we demonstrated that, at certain level of doping on carbon materials can reveal a good performance. However, increments from that level further decrease the performance. Metal loaded 1 wt.% Thiourea doped (M-CNF-T-1%) sample electrodes showed a high specific capacitance value of 207.29 F. g^{-1} at scan rate of 10 mVs^{-1}. This was ascribed to improved electrical conductivity and ion permittivity of carbon materials due to the presence of graphitic-nitrogen on carbon ring structure and nature of catalyst. Hence, the synthesized materials offer a suitable electrode material for high-performance supercapacitors.

Bibliography

Al-Enizi, A. M., Elzatahry, A. A., Abdullah, A. M., AlMaadeed, M. A., Wang, J., Zhao, D., & Al-Deyab, S. (2014). Synthesis and electrochemical properties of nickel oxide/carbon nanofiber composites. *Carbon*, *71*, 276–283. http://doi.org/10.1016/j.carbon.2014.01.052

Beese, A. M., Papkov, D., Li, S., Dzenis, Y., & Espinosa, H. D. (2013). In situ transmission electron microscope tensile testing reveals structure-property relationships in carbon nanofibers. *Carbon*, *60*, 246–253. http://doi.org/10.1016/j.carbon.2013.04.018

Bhagwan, J., Sahoo, A., Yadav, K. L., & Sharma, Y. (2015). Porous, One dimensional and High Aspect Ratio Mn3O4 Nanofibers: Fabrication and Optimization for Enhanced Supercapacitive Properties. *Electrochimica Acta*, *174*, 992–1001. http://doi.org/10.1016/j.electacta.2015.06.073

Cai, J., Niu, H., Li, Z., Du, Y., Cizek, P., Xie, Z., … Lin, T. (2015). High-Performance Supercapacitor Electrode Materials from Cellulose-Derived Carbon Nanofibers. *ACS Applied Materials & Interfaces*, *7*(27), 14946–14953. http://doi.org/10.1021/acsami.5b03757

Candelaria, S. L., Shao, Y., Zhou, W., Li, X., Xiao, J., Zhang, J. G., … Cao, G. (2012). Nanostructured carbon for energy storage and conversion. *Nano Energy*, *1*(2), 195–220. http://doi.org/10.1016/j.nanoen.2011.11.006

Cao, Y., Lin, B., Sun, Y., Yang, H., & Zhang, X. (2015). Sr-doped Lanthanum Nickelate Nano fi bers for High Energy Density Supercapacitors. *Electrochimica Acta*, *174*, 41–50. http://doi.org/10.1016/j.electacta.2015.05.131

Chen, J. C., & Harrison, I. R. (2002). Modification of polyacrylonitrile (PAN) carbon fiber precursor via post-spinning plasticization and stretching in dimethyl formamide (DMF). *Carbon*, *40*(1), 25–45. http://doi.org/10.1016/S0008-6223(01)00050-1

Chen, L., Cui, X., Wang, M., Du, Y., Zhang, X., Wan, G., … Shi, J. (2015). Microwave-Assisted Synthesis of Co-Coordinated Hollow Mesoporous Carbon Cubes for Oxygen Reduction Reactions. *Langmuir*, *31*(27), 7644–7651. http://doi.org/10.1021/acs.langmuir.5b01256

Chen, L., Zhang, X., Liang, H., Kong, M., Guan, Q., Chen, P., & Al, C. E. T. (2012). Synthesis of Nitrogen-Doped Porous Carbon Nano fi bers as an E ffi cient Electrode Material for Supercapacitors, (8), 7092–7102.

Chen, S., He, S., & Hou, H. (2013). Electrospinning technology for applications in supercapacitors. *Current Organic Chemistry*, *17*(13), 1402–1410. http://doi.org/10.2174/1385272811317130007

Chen, S., Ma, W., Cheng, Y., Weng, Z., Sun, B., Wang, L., … Cheng, H.-M. (2015). Scalable non-liquid-crystal spinning of locally aligned graphene fibers for high-performance wearable supercapacitors. *Nano Energy*, *15*, 642–653.

http://doi.org/10.1016/j.nanoen.2015.05.004

Chen, T., & Dai, L. (2013). Carbon nanomaterials for high-performance supercapacitors. *Materials Today*, *16*(7-8), 272–280. http://doi.org/10.1016/j.mattod.2013.07.002

Chen, W., Fan, Z., Gu, L., Bao, X., & Wang, C. (2010). Enhanced capacitance of manganese oxide via confinement inside carbon nanotubes. *Chemical Communications (Cambridge, England)*, *46*(22), 3905–3907. http://doi.org/10.1039/c000517g

Cheng, Y., Huang, L., Xiao, X., Yao, B., Yuan, L., Li, T., … Zhou, J. (2015). Flexible and cross-linked N-doped carbon nanofiber network for High performance Freestanding supercapacitor electrode. *Nano Energy*, *15*, 66–74. http://doi.org/10.1016/j.nanoen.2015.04.007

Choi, B. G., Yang, M., Hong, W. H., Choi, J. W., & Huh, Y. S. (2012). 3D macroporous graphene frameworks for supercapacitors with high energy and power densities. *ACS Nano*, *6*(5), 4020–4028. http://doi.org/10.1021/nn3003345

Choi, H. J., Jung, S. M., Seo, J. M., Chang, D. W., Dai, L., & Baek, J. B. (2012). Graphene for energy conversion and storage in fuel cells and supercapacitors. *Nano Energy*, *1*(4), 534–551. http://doi.org/10.1016/j.nanoen.2012.05.001

Dalton, S., Heatley, F., & Budd, P. M. (1999). Thermal stabilization of polyacrylonitrile fibres. *Polymer*, *40*(20), 5531–5543. http://doi.org/10.1016/S0032-3861(98)00778-2

Dong, Q., Wang, G., Hu, H., Yang, J., Qian, B., Ling, Z., & Qiu, J. (2013). Ultrasound-

assisted preparation of electrospun carbon nano fi ber / graphene composite electrode for supercapacitors. *Journal of Power Sources*, *243*, 350–353. http://doi.org/10.1016/j.jpowsour.2013.06.060

Egorysheva, A. V., Gaitko, O. M., Rudnev, P. O., Kuvshinova, T. B., & Yapryntsev, A. D. (2015). Crystallization in the Bi2O3-Fe2O3-NaOH system upon microwave-assisted hydrothermal synthesis. *Russian Journal of Inorganic Chemistry*, *60*(11), 1304–1310. http://doi.org/10.1134/S0036023615110042

Frackowiak, E. (2007). Carbon materials for supercapacitor application. *Physical Chemistry Chemical Physics*, *9*(15), 1774–1785. http://doi.org/10.1039/b618139m

Frackowiak, E., & Béguin, F. (2001). Carbon materials for the electrochemical storage of energy in capacitors. *Carbon*, *39*(6), 937–950. http://doi.org/10.1016/S0008-6223(00)00183-4

Fu, Z., Li, X., & Xu, G. (2014). Novel electrospun SnO\n 2\n @carbon nanofibers as high performance anodes for lithium-ion batteries. *Crystal Research and Technology*, *49*(7), 441–445. http://doi.org/10.1002/crat.201300211

Gao, Y., Presser, V., Zhang, L., Niu, J. J., McDonough, J. K., Pérez, C. R., … Gogotsi, Y. (2012). High power supercapacitor electrodes based on flexible TiC-CDC nano-felts. *Journal of Power Sources*, *201*, 368–375. http://doi.org/10.1016/j.jpowsour.2011.10.128

Ghouri, Z. K., Barakat, N. A. M., Alam, A., Park, M., & Han, T. H. (2015). Facile

synthesis of Fe / CeO 2 -doped CNFs and Their Capacitance Behavior. *International Journal of ELECTROCHEMICAL SCIENCE*, *10*, 2064–2071.

Hao, L., Li, X., & Zhi, L. (2013). Carbonaceous electrode materials for supercapacitors. *Advanced Materials*, *25*(28), 3899–3904. http://doi.org/10.1002/adma.201301204

He, S., Chen, L., Xie, C., Hu, H., Chen, S., Hanif, M., & Hou, H. (2013). Supercapacitors based on 3D network of activated carbon nanowhiskers wrapped-on graphitized electrospun nanofibers. *Journal of Power Sources*, *243*, 880–886. http://doi.org/10.1016/j.jpowsour.2013.06.104

Hsu, H., Wang, C., Chang, Y., Hu, J., Yao, B., & Lin, C. (2015). Graphene oxides and carbon nanotubes embedded in poly- acrylonitrile-based carbon nano fi bers used as electrodes for supercapacitor. *Journal of Physical and Chemistry of Solids*, *85*, 62–68. http://doi.org/10.1016/j.jpcs.2015.04.010

Hu, C.-C., Chang, K.-H., & Wang, C.-C. (2007). Two-step hydrothermal synthesis of Ru–Sn oxide composites for electrochemical supercapacitors. *Electrochimica Acta*, *52*(13), 4411–4418. http://doi.org/10.1016/j.electacta.2006.12.022

Huang, K., Yao, Y., Yang, X., Chen, Z., & Li, M. (2016). Fabrication of flexible hierarchical porous nitrogen-doped carbon nanofiber films for application in binder-free supercapacitors. *Materials Chemistry and Physics*, *169*, 1–5. http://doi.org/10.1016/j.matchemphys.2015.11.024

Huang, Z. M., Zhang, Y. Z., Kotaki, M., & Ramakrishna, S. (2003). A review on polymer

nanofibers by electrospinning and their applications in nanocomposites. *Composites Science and Technology*, *63*(15), 2223–2253. http://doi.org/10.1016/S0266-3538(03)00178-7

Inagaki, M., Yang, Y., & Kang, F. (2012). Carbon nanofibers prepared via electrospinning. *Advanced Materials*, *24*(19), 2547–2566. http://doi.org/10.1002/adma.201104940

Jing, M., Wang, C. guo, Wang, Q., Bai, Y. jun, & Zhu, B. (2007). Chemical structure evolution and mechanism during pre-carbonization of PAN-based stabilized fiber in the temperature range of 350-600 ??C. *Polymer Degradation and Stability*, *92*(9), 1737–1742. http://doi.org/10.1016/j.polymdegradstab.2007.05.020

Jodeh, S. (2008). Chemical structural characterization of pyrolyzed and subsequently ion-implanted poly(acrylonitrile). *Journal of Analytical and Applied Pyrolysis*, *82*(2), 235–239. http://doi.org/10.1016/j.jaap.2008.03.014

Kiciński, W., Szala, M., & Bystrzejewski, M. (2014). Sulfur-doped porous carbons: Synthesis and applications. *Carbon*, *68*(MARCH 2014), 1–32. http://doi.org/10.1016/j.carbon.2013.11.004

Kim, B. H., Seung Yang, K., & Woo, H. G. (2013). Boron-nitrogen functional groups on porous nanocarbon fibers for electrochemical supercapacitors. *Materials Letters*, *93*, 190–193. http://doi.org/10.1016/j.matlet.2012.11.057

Kim, B.-H., Kim, C. H., & Lee, D. G. (2016). Mesopore-enriched activated carbon

nanofiber web containing RuO2 as electrode material for high-performance supercapacitors. *Journal of Electroanalytical Chemistry*, *760*, 64–70. http://doi.org/10.1016/j.jelechem.2015.12.001

Kim, B.-H., Kim, C. H., Yang, K. S., Rahy, A., & Yang, D. J. (2012). Electrospun vanadium pentoxide/carbon nanofiber composites for supercapacitor electrodes. *Electrochimica Acta*, *83*, 335–340. http://doi.org/10.1016/j.electacta.2012.07.093

Kim, S. Y., Kim, B. H., Yang, K. S., & Oshida, K. (2012). Supercapacitive properties of porous carbon nanofibers via the electrospinning of metal alkoxide-graphene in polyacrylonitrile. *Materials Letters*, *87*, 157–161. http://doi.org/10.1016/j.matlet.2012.07.093

Kolathodi, M. S., & Natarajan, T. S. (2015). Development of high-performance flexible solid state supercapacitor based on activated carbon and electrospun TiO 2 nanofibers. *Scripta Materialia*, *101*, 84–86. http://doi.org/10.1016/j.scriptamat.2015.01.024

Kumar, M., Subramania, A., & Balakrishnan, K. (2014). Preparation of electrospun Co3O4 nanofibers as electrode material for high performance asymmetric supercapacitors. *Electrochimica Acta*, *149*, 152–158. http://doi.org/10.1016/j.electacta.2014.10.021

Kundu, M., & Liu, L. (2015). Binder-free electrodes consisting of porous NiO nano fi bers directly electrospun on nickel foam for high-rate supercapacitors. *Materials*

Letters, *144*, 114–118. http://doi.org/10.1016/j.matlet.2015.01.032

Lai, C.-C., & Lo, C.-T. (2015). Effect of Temperature on Morphology and Electrochemical Capacitive Properties of Electrospun Carbon Nanofibers and Nickel Hydroxide Composites. *Electrochimica Acta*, *174*, 806–814. http://doi.org/10.1016/j.electacta.2015.06.077

Lai, F., Huang, Y., Miao, Y.-E., & Liu, T. (2015). Controllable preparation of multi-dimensional hybrid materials of nickel-cobalt layered double hydroxide nanorods/nanosheets on electrospun carbon nanofibers for high-performance supercapacitors. *Electrochimica Acta*, *174*, 456–463. http://doi.org/10.1016/j.electacta.2015.06.031

Lee, E., Lee, T., & Kim, B. S. (2014). Electrospun nanofiber of hybrid manganese oxides for supercapacitor: Relevance to mixed inorganic interfaces. *Journal of Power Sources*, *255*, 335–340. http://doi.org/10.1016/j.jpowsour.2014.01.011

Li, X., & Wei, B. (2013). Supercapacitors based on nanostructured carbon. *Nano Energy*, *2*(2), 159–173. http://doi.org/10.1016/j.nanoen.2012.09.008

Li, X.-F., Lian, K.-Y., Liu, L., Wu, Y., Qiu, Q., Jiang, J., … Luo, Y. (2016). Unraveling the formation mechanism of graphitic nitrogen-doping in thermally treated graphene with ammonia. *Scientific Reports*, *6*(October 2015), 23495. http://doi.org/10.1038/srep23495

Liu, Y., Xu, X., Lu, T., Sun, Z., Chua, D. H. C., & Pan, L. (2015). Nitrogen-doped

electrospun reduced graphene oxide–carbon nanofiber composite for capacitive deionization. *RSC Adv.*, *5*(43), 34117–34124. http://doi.org/10.1039/C5RA00620A

Lo, A.-Y., Jheng, Y., Huang, T.-C., & Tseng, C.-M. (2015). Study on RuO2/CMK-3/CNTs composites for high power and high energy density supercapacitor. *Applied Energy*, *153*, 15–21. http://doi.org/10.1016/j.apenergy.2015.04.050

Ma, W., Chen, S., Yang, S., Chen, W., Cheng, Y., Guo, Y., … Zhu, M. (2016). Hierarchical MnO2 nanowire/graphene hybrid fibers with excellent electrochemical performance for flexible solid-state supercapacitors. *Journal of Power Sources*, *306*, 481–488. http://doi.org/10.1016/j.jpowsour.2015.12.063

Madhurambal, G., Mariappan, M., & Mojumdar, S. C. (2010). Thermal , UV and FTIR spectral studies of urea – thiourea zinc chloride single crystal, 763–768. http://doi.org/10.1007/s10973-010-0758-0

Mao, X., Alan Hatton, T., & Rutledge, G. C. (2013). A review of electrospun carbon fibers as electrode materials for energy storage. *Current Organic Chemistry*, *17*(13), 1390–1401. http://doi.org/10.2174/1385272811317130006

Menéndez, J. A., Arenillas, A., Fidalgo, B., Fernández, Y., Zubizarreta, L., Calvo, E. G., & Bermúdez, J. M. (2010). Microwave heating processes involving carbon materials, *91*(1), 1–8. http://doi.org/10.1016/j.fuproc.2009.08.021

Miao, F., Shao, C., Li, X., Lu, N., Wang, K., Zhang, X., & Liu, Y. (2015). Flexible solid-state supercapacitors based on freestanding electrodes of electrospun

polyacrylonitrile@polyaniline core-shell nanofibers. *Electrochimica Acta*, *176*, 293–300. http://doi.org/10.1016/j.electacta.2015.06.141

Miao, F., Shao, C., Li, X., Lu, N., Wang, K., Zhang, X., & Liu, Y. (2016). Polyaniline-coated electrospun carbon nano fi bers with high mass loading and enhanced capacitive performance as freestanding electrodes for fl exible solid-state supercapacitors, *95*, 233–241. http://doi.org/10.1016/j.energy.2015.12.013

Mondal, K., Tsai, C.-Y., Stout, S., & Talapatra, S. (2015). Manganese oxide based hybrid nanofibers for supercapacitors. *Materials Letters*, *148*, 142–146. http://doi.org/10.1016/j.matlet.2015.02.078

Nataraj, S. K., Yang, K. S., & Aminabhavi, T. M. (2012). Polyacrylonitrile-based nanofibers - A state-of-the-art review. *Progress in Polymer Science (Oxford)*, *37*(3), 487–513. http://doi.org/10.1016/j.progpolymsci.2011.07.001

Niu, H., Zhang, J., Xie, Z., Wang, X., & Lin, T. (2011). Preparation, structure and supercapacitance of bonded carbon nanofiber electrode materials. *Carbon*, *49*(7), 2380–2388. http://doi.org/10.1016/j.carbon.2011.02.005

Pandolfo, A. G., & Hollenkamp, A. F. (2006). Carbon properties and their role in supercapacitors. *Journal of Power Sources*, *157*(1), 11–27. http://doi.org/10.1016/j.jpowsour.2006.02.065

Ra, E. J., Raymundo-Piñero, E., Lee, Y. H., & Béguin, F. (2009). High power supercapacitors using polyacrylonitrile-based carbon nanofiber paper. *Carbon*,

47(13), 2984–2992. http://doi.org/10.1016/j.carbon.2009.06.051

Rahaman, M. S. A., Ismail, A. F., & Mustafa, A. (2007). A review of heat treatment on polyacrylonitrile fiber. *Polymer Degradation and Stability*, *92*(8), 1421–1432. http://doi.org/10.1016/j.polymdegradstab.2007.03.023

Raj, B. G. S., Ramprasad, R. N. R., Asiri, A. M., Wu, J. J., & Anandan, S. (2015). Ultrasound assisted synthesis of Mn3O4 nanoparticles anchored graphene nanosheets for supercapacitor applications. *Electrochimica Acta*, *156*, 127–137. http://doi.org/10.1016/j.electacta.2015.01.052

Ren, Y., Dai, J., Pang, B., Liu, X., & Yu, J. (2015). Synergistic enhancement of electrochemical performance of electrospun TiC/C hybrid nanofibers for supercapacitor application. *Electrochimica Acta*, *176*, 402–409. http://doi.org/10.1016/j.electacta.2015.07.025

Reneker, D. H., & Yarin, A. L. (2008). Electrospinning jets and polymer nanofibers. *Polymer*, *49*(10), 2387–2425. http://doi.org/10.1016/j.polymer.2008.02.002

Shao, J., Li, W., Zhou, X., & Hu, J. (2014). Magnetic-field-assisted hydrothermal synthesis of 2 x 2 tunnels of MnO2 nanostructures with enhanced supercapacitor performance. *CrystEngComm*, *16*(43), 9987–9991. http://doi.org/10.1039/c4ce01385a

Shi, X., Zhou, W., Ma, D., Ma, Q., Bridges, D., Ma, Y., & Hu, A. (2015). Electrospinning of Nanofibers and Their Applications for Energy Devices. *Journal*

of Nanomaterials, *2015*. http://doi.org/10.1155/2015/140716

Staaf, L. G. H., Lundgren, P., & Enoksson, P. (2014). Present and future supercapacitor carbon electrode materials for improved energy storage used in intelligent wireless sensor systems. *Nano Energy*, *9*, 128–141. http://doi.org/10.1016/j.nanoen.2014.06.028

Tai, Z., Yan, X., Lang, J., & Xue, Q. (2012). Enhancement of capacitance performance of flexible carbon nanofiber paper by adding graphene nanosheets. *Journal of Power Sources*. http://doi.org/10.1016/j.jpowsour.2011.10.009

Tang, K., Li, Y., Cao, H., Su, C., Zhang, Z., & Zhang, Y. (2016). Amorphous-crystalline TiO2/carbon nanofibers composite electrode by one-step electrospinning for symmetric supercapacitor. *Electrochimica Acta*, *190*, 678–688. http://doi.org/10.1016/j.electacta.2015.12.209

Thangappan, R., Kalaiselvam, S., Elayaperumal, A., & Jayavel, R. (2014). Synthesis of graphene oxide/vanadium pentoxide composite nanofibers by electrospinning for supercapacitor applications. *Solid State Ionics*, *268*(PB), 321–325. http://doi.org/10.1016/j.ssi.2014.10.025

Tian, X., Zhao, N., Song, Y., Wang, K., Xu, D., Li, X., … Liu, L. (2015). Synthesis of nitrogen-doped electrospun carbon nanofibers with superior performance as efficient supercapacitor electrodes in alkaline solution. *Electrochimica Acta*, *185*, 40–51. http://doi.org/10.1016/j.electacta.2015.10.096

Tsubota, T., Takenaka, K., Murakami, N., & Ohno, T. (2011). Performance of nitrogen- and sulfur-containing carbon material derived from thiourea and formaldehyde as electrochemical capacitor. *Journal of Power Sources*, *196*(23), 10455–10460. http://doi.org/10.1016/j.jpowsour.2011.07.025

van Schalkwijk W. (2005). Nanostructured Materials for Advanced Energy Conversion and Storage Devices. *Nat. Mater.*, *4*(May), 366.

Vangari, M., Pryor, T., & Jiang, L. (2013). Supercapacitors: Review of materials and fabrication methods. *Journal of Energy Engineering*, *139*(2), 72–79. http://doi.org/10.1061/(ASCE)EY.1943-7897.0000102.

Vidhyadharan, B., Zain, N. K. M., Misnon, I. I., Aziz, R. A., Ismail, J., Yusoff, M. M., & Jose, R. (2014). High performance supercapacitor electrodes from electrospun nickel oxide nanowires. *Journal of Alloys and Compounds*, *610*, 143–150. http://doi.org/10.1016/j.jallcom.2014.04.211

Vidyadharan, B., Aziz, R. A., Misnon, I. I., Anil Kumar, G. M., Ismail, J., Yusoff, M. M., & Jose, R. (2014). High energy and power density asymmetric supercapacitors using electrospun cobalt oxide nanowire anode. *Journal of Power Sources*, *270*, 526–535. http://doi.org/10.1016/j.jpowsour.2014.07.134

Vidyadharan, B., Misnon, I. I., Ismail, J., Yusoff, M. M., & Jose, R. (2015). High performance asymmetric supercapacitors using electrospun copper oxide nanowires anode. *Journal of Alloys and Compounds*, *633*, 22–30.

http://doi.org/10.1016/j.jallcom.2015.01.278

Wang, J., Zhang, X., Wei, Q., Lv, H., Tian, Y., Tong, Z., … Mai, L. (2016). 3D self-supported nanopine forest-like Co3O4@CoMoO4 core–shell architectures for high-energy solid state supercapacitors. *Nano Energy*, *19*, 222–233. http://doi.org/10.1016/j.nanoen.2015.10.036

Wang, Y., Li, S., Hsiao, S., Liao, W., Chen, P., Yang, S., … Ma, C. M. (2014). Integration of tailored reduced graphene oxide nanosheets and electrospun polyamide-66 nanofabrics for a flexible supercapacitor with high-volume- and high-area-specific capacitance. *Carbon*, *73*, 87–98. http://doi.org/10.1016/j.carbon.2014.02.043

Wangxi, Z., Jie, L., & Gang, W. (2003). Evolution of structure and properties of PAN precursors during their conversion to carbon fibers. *Carbon*, *41*(14), 2805–2812. http://doi.org/10.1016/S0008-6223(03)00391-9

Wei, K., Kim, K.-O., Song, K.-H., Kang, C.-Y., Lee, J. S., Gopiraman, M., & Kim, I.-S. (2016). Nitrogen- and Oxygen-Containing Porous Ultrafine Carbon Nanofiber: A Highly Flexible Electrode Material for Supercapacitor. *Journal of Materials Science & Technology*. http://doi.org/10.1016/j.jmst.2016.03.014

Xu, P., Kang, J., Choi, J. B., Suhr, J., Yu, J., Li, F., … Chou, T. W. (2014). Laminated ultrathin chemical vapor deposition graphene films based stretchable and transparent high-rate supercapacitor. *ACS Nano*, *8*(9), 9437–9445.

http://doi.org/10.1021/nn503570j

Xu, Q., Yu, X., Liang, Q., Bai, Y., Huang, Z.-H., & Kang, F. (2015). Nitrogen-doped hollow activated carbon nanofibers as high performance supercapacitor electrodes. *Journal of Electroanalytical Chemistry*, *739*, 84–88. http://doi.org/10.1016/j.jelechem.2014.12.027

Xu, Y., Wang, J., Shen, L., Dou, H., & Zhang, X. (2015). One-Dimensional Vanadium Nitride Nanofibers Fabricated by Electrospinning for Supercapacitors. *Electrochimica Acta*, *173*, 680–686. http://doi.org/10.1016/j.electacta.2015.05.088

Yang, J. E., Jang, I., Kim, M., Baeck, S. H., Hwang, S., & Shim, S. E. (2013). Electrochemically polymerized vine-like nanostructured polyaniline on activated carbon nanofibers for supercapacitor. *Electrochimica Acta*, *111*, 136–143. http://doi.org/10.1016/j.electacta.2013.07.183

Yang, W., Ni, M., Ren, X., Tian, Y., Li, N., Su, Y., & Zhang, X. (2015). Graphene in Supercapacitor Applications. *Current Opinion in Colloid and Interface Science*, *20*(5-6), 416–428. http://doi.org/10.1016/j.cocis.2015.10.009

Yarin, A. L., Koombhongse, S., & Reneker, D. H. (2001). Taylor cone and jetting from liquid droplets in electrospinning of nanofibers. *Journal of Applied Physics*, *90*(9), 4836–4846. http://doi.org/10.1063/1.1408260

Yu, A., Chen, Z., Maric, R., Zhang, L., Zhang, J., & Yan, J. (2015). Electrochemical supercapacitors for energy storage and delivery: Advanced materials, technologies

and applications. *Applied Energy*, *153*, 1–2. http://doi.org/10.1016/j.apenergy.2015.05.054

Yu, G., Xie, X., Pan, L., Bao, Z., & Cui, Y. (2013). Hybrid nanostructured materials for high-performance electrochemical capacitors. *Nano Energy*, *2*(2), 213–234. http://doi.org/10.1016/j.nanoen.2012.10.006

Yu, Z., Tetard, L., Zhai, L., & Thomas, J. (2015). Supercapacitor electrode materials: nanostructures from 0 to 3 dimensions. *Energy & Environmental Science*, *8*(3), 702–730. http://doi.org/10.1039/C4EE03229B

Zeng, J., Cao, Q., Wang, X., Jing, B., Peng, X., & Tang, X. (2015). Nitrogen-doped hierarchical porous carbon for supercapacitor with well electrochemical performances. *Journal of Solid State Electrochemistry*, *19*(6), 1591–1597. http://doi.org/10.1007/s10008-015-2776-0

Zhang, B., Kang, F., Tarascon, J.-M., & Kim, J.-K. (2015). Recent Advances in Electrospun Carbon Nanofibers and Their Application in Electrochemical Energy Storage. *Progress in Materials Science*, *76*, 319–380. http://doi.org/10.1016/j.pmatsci.2015.08.002

Zhang, D., Karki, A. B., Rutman, D., Young, D. P., Wang, A., Cocke, D., … Guo, Z. (2009). Electrospun polyacrylonitrile nanocomposite fibers reinforced with Fe3O4 nanoparticles: Fabrication and property analysis. *Polymer*, *50*(17), 4189–4198. http://doi.org/10.1016/j.polymer.2009.06.062

Zhang, L., Aboagye, A., Kelkar, A., Lai, C., & Fong, H. (2014). A review: Carbon nanofibers from electrospun polyacrylonitrile and their applications. *Journal of Materials Science*, *49*(2), 463–480. http://doi.org/10.1007/s10853-013-7705-y

Zhang, L. L., Zhou, R., & Zhao, X. S. (2009). Carbon-based materials as supercapacitor electrodes. *Journal of Materials Chemistry*, *38*(29), 2520–2531. http://doi.org/10.1039/c000417k

Zhao, G., Chen, B., & Qian, S. (1992). Kinetics of the -C = N bond transformation into the conjugated \ C = N- bond in acrylonitrile copolymer using in situ Fo & ier transform infrared spectroscopy. *Science*, *23*, 87–97. http://doi.org/10.1016/0165-2370(92)80015-E

Zhao, X., Du, Y., Li, Y., & Zhang, Q. (2015). Encapsulation of manganese oxides nanocrystals in electrospun carbon nano fi bers as free-standing electrode for supercapacitors. *Ceramics International*, *41*(6), 7402–7410. http://doi.org/10.1016/j.ceramint.2015.02.053

Zhao, X., Zhang, Q., Chen, C. M., Zhang, B., Reiche, S., Wang, A., … Sheng Su, D. (2012). Aromatic sulfide, sulfoxide, and sulfone mediated mesoporous carbon monolith for use in supercapacitor. *Nano Energy*, *1*(4), 624–630. http://doi.org/10.1016/j.nanoen.2012.04.003

Zhi, M., Manivannan, A., Meng, F., & Wu, N. (2012). Highly conductive electrospun carbon nanofiber/MnO2 coaxial nano-cables for high energy and power density

supercapacitors. *Journal of Power Sources*, *208*, 345–353. http://doi.org/10.1016/j.jpowsour.2012.02.048

Zhou, D., Lin, H., Zhang, F., Niu, H., Cui, L., Wang, Q., & Qu, F. (2015). Freestanding MnO2 nanoflakes/porous carbon nanofibers for high-performance flexible supercapacitor electrodes. *Electrochimica Acta*, *161*, 427–435. http://doi.org/10.1016/j.electacta.2015.02.085

Zhou, Z., & Wu, X. (2014). High-performance porous electrodes for pseudosupercapacitors based on graphene-beaded carbon nano fi bers surface-coated with nanostructured conducting polymers. *Journal of Power Sources*, *262*, 44–49. http://doi.org/10.1016/j.jpowsour.2014.03.096

Zhou, Z., & Wu, X. F. (2013). Graphene-beaded carbon nanofibers for use in supercapacitor electrodes: Synthesis and electrochemical characterization. *Journal of Power Sources*, *222*, 410–416. http://doi.org/10.1016/jjpowsour.2012.09.004

Zhu, L., Sun, H., Fu, H., Zheng, J., Zhang, N., Li, Y., & Chen, B. H. (2015). Effect of ruthenium nickel bimetallic composition on the catalytic performance for benzene hydrogenation to cyclohexane. *Applied Catalysis A: General*, *499*, 124–132. http://doi.org/10.1016/j.apcata.2015.04.016